Polymeric membranes for CO_2 separation and capture

Yang Han [a], W.S. Winston Ho [a,b,*]

[a] *William G. Lowrie Department of Chemical and Biomolecular Engineering, The Ohio State University, 151 West Woodruff Avenue, Columbus, OH 43210-1350, USA*

[b] *Department of Materials Science and Engineering, The Ohio State University, 2041 College Road, Columbus, OH 43210-1178, USA*

* Corresponding author. Tel.: +1 614 292 9970; fax: +1 614 292 3769.

E-mail address: ho.192@osu.edu (W.S.W. Ho).

Abstract

Over the past decade, CO_2 separation and capture have become the new bandwagon for polymer science and membrane research. This review presents the fundamentals of CO_2/gas separation in polymeric membranes and discusses how these principles underpin opportunities and challenges for post-combustion carbon capture (CO_2/N_2), hydrogen purification (CO_2/H_2), and natural gas and biogas sweetening (CO_2/CH_4). Emerging polymeric membrane materials are discussed, including a few polymers containing a high content of polar functional groups (i.e., ether oxygen-rich polymers and polymeric ionic liquids), shape-persisting glassy polymers (i.e., perfluoropolymers, thermally rearranged polymers, iptycene-containing polymers), and reactive polymers featuring facilitated transport. Moreover, the promising candidates for each CO_2 separation application are highlighted. Finally, the permeability-selectivity data reviewed were plotted against their 2008 and 2019 upper bounds.

Keywords: Carbon capture; hydrogen purification; natural gas sweetening; polymeric membrane; gas separation

1. Introduction

The first commercial membrane gas separation system was developed by Monsanto in 1979 for the separation of H_2 from CH_4, N_2, and Ar in purge gases in ammonia and chemical plants and refineries [1,2]. Since then, a number of other applications were established, including air separation by Generon (1982), H_2 purification in synthesis gas plants by Ube Industries (1987), and natural gas treatment by UOP (1994) [3-5]. The rapid growth of membrane market was driven by advances in polymer science and membrane process engineering. Compared to other purification processes, membrane is known for its system compactness, energy efficiency, operational simplicity, and ability to overcome thermodynamic limitations [6]. These advantages quickly attracted the interests from academia and industry in early 2000s when the CO_2 emissions from the use of fossil fuels became a pressing social and environmental issue [7-11]. In 2019 alone, fossil fuels accounted for about 80% of the energy production in the United States and contributed to approximately 1616 million metric tonne of carbon emissions [12]. Carbon dioxide separation and capture could be the next opportunity for the large-scale deployment of gas separation membranes.

Membrane-based carbon capture is best suited for emissions from large stationary sources. Based on the location, these applications can be divided into three categories: (1) CO_2/N_2 separation from flue gases, (2) CO_2/H_2 separation in syngas processing, and (3) CO_2/CH_4 separation in natural gas and biogas sweetening. Aside from the dissimilar gas pairs, these separation scenarios differ significantly in the CO_2 concentration, pressure, major contaminants, and separation specifications.

In post-combustion carbon capture, the flue gases are discharged at ambient conditions with 11–14% CO_2 from coal-fired power plants and 4–8% CO_2 from natural gas combined cycle power

plants [13,14]. Besides N_2, flue gases also contain water, O_2, and trace amounts of SO_x and NO_x. Because of the low CO_2 partial pressure, a highly CO_2-permeable yet highly selective membrane is needed to achieve a deep carbon cleaning [15,16]. In addition, since the CO_2 captured and low-purity N_2 are the byproducts, membrane process does not have the luxury of producing a high-value product to rebate its capital and operational costs.

In comparison, in pre-combustion carbon, there is a much more favorable syngas composition of ca. 40% CO_2 and 56% H_2 with balance of water, CO, H_2S, etc., at a temperature of approximately 240°C and a pressure as high as 50 atm [17-19]. The high transmembrane driving force relaxes the requirement for a highly-permeable membrane, but the membrane material needs to exhibit a high CO_2 or H_2 selectivity at a high temperature in order to reduce the H_2 loss and avoid a significant syngas cooling.

Depending on the geographical location, crude natural gas contains 5–70% CO_2, and membrane separation is typically performed at ambient temperature with a pressure of 30–60 atm [20]. Often, membrane-based dehydration and desulfurization are carried out prior to the CO_2 removal in order to avoid the condensation of acidic water caused by the Joule–Thomson effect [21,22]. In addition, the membrane material should be resistant to plasticization of CO_2 and hydrocarbon vapors. These challenges imposed by the high natural gas pressure are absent for biogas, which typically consists of 38–40% CO_2, 55–60% CH_4, and 1–2% water at atmospheric pressure [23]. However, the membrane should have a sufficient CO_2 permeance due to the reduced driving force.

For these CO_2 separation applications, the drastically different operating conditions also impose different challenges on the membrane material development. In CO_2/N_2 separation, the chemical properties of polymers are altered to promote the CO_2 sorption and thus separate this gas

pair in similar molecular size. The synthesis of CO_2-philic functional polymers is a prominent research area, for which various Lewis bases are often incorporated for their favorable physical interaction (e.g., ether and carbonyl oxygens) [24,25] or chemical reaction (e.g., amines) [26,27] with CO_2. Contrarily, the tuning of polymer conformation is more important than the chemical functionality for the size-sieving, H_2-selective membranes [28,29]. This is in particular the case for syngas purification, where the CO_2 sorption is largely suppressed by the high operating temperature [30]. For natural gas processing, the high CO_2 partial pressure and the presence of heavy hydrocarbons can cause many non-ideal effects, such as the CO_2-induced plasticization and membrane swelling [31]. These effects often increase the interchain spacing and lead to a significantly reduced CO_2/CH_4 selectivity. Therefore, the membrane development pivots on the synthesis of shape-persisting polymers with high chain rigidity.

In the past decade, significant progress has been witnessed in membrane science, and new classes of polymers have been developed with improved performance for CO_2 separation and capture. This paper first discusses the fundamental scientific principles for CO_2/gas separation in polymeric membranes. Emerging polymeric materials are then highlighted, including ether oxygen-rich polymers, polymeric ionic liquids, perfluoropolymers, thermally rearranged polymers, iptycene-containing polymers, some other noteworthy non-reactive polymers, and reactive polymers based on facilitated transport. Finally, the opportunities and challenges of these emerging materials are summarized for different CO_2/gas separation applications.

2. Theory and Terminology

2.1. Light gas permeation in non-reactive polymers

As a pressure-driven process, membrane separation requires a transmembrane pressure differential for the permeation of light gases (e.g., CO_2, N_2, H_2, and CH_4). The steady-state permeance of a polymeric membrane to a gaseous species i is defined as:

$$\frac{P_i}{\ell} = \frac{J_i}{\Delta p_i} \tag{1}$$

where P_i/ℓ, J_i, and Δp_i are the permeance, flux, and transmembrane partial pressure differential of species i. The permeance reflects the mass transfer resistance in the permeation through the membrane, which is typically reported in Gas Permeation Unit (GPU, 1 GPU = 1×10^{-6} cm^3(STP) cm^{-2} s^{-1} $cmHg^{-1}$). The intrinsic conductance of the polymer can then be calculated by multiplying the permeance with the membrane thickness (ℓ), which is defined as the gas permeability coefficient (P_i) with a unit of Barrer (1 Barrer = 1×10^{-10} cm^3(STP) cm cm^{-2} s^{-1} $cmHg^{-1}$).

The permeability is a material property, which is usually measured by using a free-standing film with a thickness of a few hundred microns. The permeance, however, is a membrane property that depends on the membrane thickness and configuration [32-35]. For a non-reactive polymer with certain gas permeability, a higher permeance can be achieved by reducing the membrane thickness. Therefore, the formation of thin membrane is important for practical membrane applications.

For non-reactive polymers, the transport of gas molecules typically follows the solution-diffusion mechanism, and the permeability coefficient is usually given by:

$$P_i = S_i \times D_i \tag{2}$$

where S_i and D_i are the solubility and diffusivity coefficients of species i in the polymer, respectively [2,36]. The ideal selectivity of species i over species j is the ratio of their pure-gas or mixed-gas permeabilities:

$$\alpha_{ij} = \frac{P_i}{P_j} = \left(\frac{S_i}{S_j}\right)\left(\frac{D_i}{D_j}\right) \tag{3}$$

where S_i/S_j is the solubility selectivity and D_i/D_j is the diffusivity selectivity. Therefore, the separation arises from the difference in the solubilities or diffusivities of the gas pair in the polymer.

The solvation of gas molecules into a polymer is often an enthalpy-driven process. The solubility is determined by its condensability and correlates with its Lennard-Jones temperature (ε_i/k) as:

$$\ln S_i = M + N\frac{\varepsilon_i}{k} - \left(500 - 10\frac{\varepsilon_i}{k}\right)\left(\frac{1}{T} - \frac{1}{298}\right) \tag{4}$$

where M and N are constants and T is the absolute temperature [24,37]. Robeson et al. reviewed a large collection of glassy and rubbery polymers, and the fitting of Eq. (4) to the solubility data at 25–35°C led to a value of –7.30 for M and 0.0249 for N (with solubility in unit of cm^3(STP) cm^{-3} $cmHg^{-1}$) [38]. The Lennard-Jones temperatures of relevant light gases are summarized in Table 1. Based on Eq. (4), the solubility coefficients can be estimated, and the solubility selectivities of CO_2 vs. other gases are also listed in Table 1. As seen, CO_2 exhibits a higher solubility than H_2 and N_2, which renders favorable CO_2 solubility selectivities over H_2 and N_2 in most polymers. However, CO_2 is only moderately more condensable than CH_4, resulting in an appreciable but lower CO_2/CH_4 solubility selectivity.

Table 1. Physical properties of light gases in non-reactive polymers and the estimated solubility and diffusivity selectivities against CO_2 at 25°C.

Gas	ε_i/k (K) [37]	S_i (cm^3(STP) cm^{-3} $cmHg^{-1}$)†	S_{CO_2}/S_i	d_i (Å) [39]	D_{CO_2}/D_i‡
H_2	59.7	3.0	29.0	2.89	0.18
CO_2	195.2	87	–	3.30	–
N_2	71.4	4.0	21.8	3.64	4.84
CH_4	148.6	27	3.20	3.80	10.7

† Estimated based on Eq. (4).
‡ Estimated based on Eq. (8) with a = 0.64 and c = 1100 cal mol^{-1} $Å^{-2}$.

The sorbed light gas molecules occupy the voids in the polymer, and they can then migrate into voids above a critical size by random volume fluctuation [40]. The gas diffusion in a weakly interacting polymer is a thermally activated process and obeys the Arrhenius equation:

$$D_i = D_{0,i} \cdot \exp\left(-\frac{E_{D,i}}{RT}\right) \tag{5}$$

where $D_{0,i}$ is a pre-exponential factor, $E_{D,i}$ the activation energy of diffusion, and R the gas constant [41]. The pre-exponential factor and the activation energy often observe a "linear free energy relation":

$$\ln D_{0,i} = a\frac{E_{D,i}}{RT} - b \tag{6}$$

where the parameters a ($a < 1$) and b are independent of the gas species [42]. The activation energy is related to the kinetic size (d_i) of the gas molecule as:

$$E_{D,i} = c\, d_i^2 - f \tag{7}$$

where c and f are constants depending on the polymer type [43]. The combination of Eqs. (5)–(7) gives a correlation between the diffusivity selectivity and the kinetic sizes of the gas pair as:

$$\ln\frac{D_i}{D_i} = \left(\frac{1-a}{RT}\right) c\left(d_j^2 - d_i^2\right) \tag{8}$$

The kinetic diameters of several light gases and the estimated diffusivity selectivities of CO_2 vs. other gases are also summarized in Table 1. The CO_2/H_2 diffusivity selectivity is less than unity, which offsets the favorable CO_2/H_2 solubility selectivity. Therefore, the common strategy for the separation of this gas pair is to operate a H_2-selective membrane, such as polyimide and polybenzimidazole (PBI), at a high temperature where the difference in the condensability is weakened [44,45]. CO_2 does not exhibit an appreciable diffusivity selectivity over N_2. Actually, CO_2 has a smaller kinetic diameter (3.30 vs. 3.64 Å) but a larger critical volume (93.9 vs. 89.8 cm^3 mol^{-1} [37]) than those of N_2, resulting in a CO_2/N_2 diffusivity selectivity near unity in most polymers [32]. For this reason, nearly all CO_2/N_2 separation membranes rely on the enhanced CO_2–polymer interaction to exhibit certain solubility selectivity. On the contrary, CO_2 has a pronounced diffusivity selectivity as well as a moderate solubility selectivity against CH_4. Most state-of-the-art CO_2/CH_4 separation membranes are glassy polymers with size-sieving ability [46].

2.2. Permeability/selectivity trade-off and upper bounds

Since the advent of commercial gas separation membranes in the late 1970s, the studies of how the polymer structure relates to the separation performance remain as the core of membrane research. Numerous analyses of structure-property data of polymeric membranes made it apparent that a trade-off exists between the permeability and selectivity [47-49]. This observation is best represented by a conceptual "upper bound" where all permeability-selectivity data are below an empirical line on a log-log scale [50]. Figure 1 shows an example of CO_2/N_2 upper bound, which was proposed by Robeson in 2008 [51]. The upper bound takes the form:

$$\alpha_{ij} = \frac{\beta_{ij}}{P_i^{\lambda_{ij}}} \tag{9}$$

where the parameters β_{ij} and λ_{ij} are for a specific gas pair and i is the more permeable species. As new polymers were synthesized and the gas separation characteristics became available, updated upper bounds were published. For instance, Comesaña-Gándara et al. revised the 2008 CO_2/N_2 upper bound in 2019 based on a series of ultra-permeable iptycene-based polymers of intrinsic microporosity (PIMs) [52]. The shift, however, was mainly reflected in a larger value of β_{ij} rather than a significant change in the slope of the upper bound (i.e., λ_{ij}).

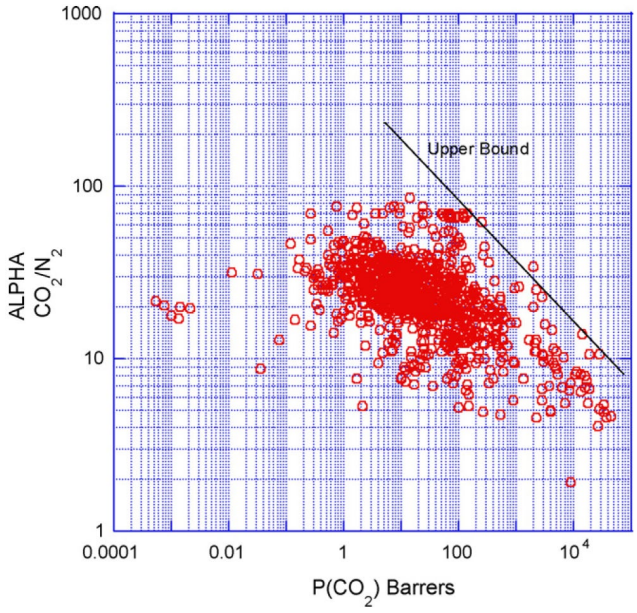

Figure 1. Experimental data of CO_2/N_2 separation and an empirical upper bound proposed by Robeson in 2008. Adapted from Ref. [51]; copyright Elsevier.

Although the upper bound is an empirical correlation, theoretical analysis has been carried out by Freeman et al. to justify and predict the position and slope of the upper bound [40,53]. In their theory, the slope is correlated to the kinetic sizes of the gas pair by the activation energy theory:

$$\lambda_{ij} = \left(\frac{d_j}{d_i}\right)^2 - 1 \tag{10}$$

and β_{ij} is expressed as:

$$\beta_{ij} = \left(\frac{S_i}{S_j}\right) S_i^{\lambda_{ij}} \cdot \exp\left\{-\lambda_{ij}\left[b - f\left(\frac{1-a}{RT}\right)\right]\right\} \tag{11}$$

where S_i and S_j are given by Eq. (4) [53]. Apparently, λ_{ij} is only a function of the kinetic sizes of the gas pair but β_{ij} is dependent on the temperature.

Exemplary upper bound behaviors at temperatures ranging from 200–400 K are shown in Figure 2 for CO_2/N_2, CO_2/CH_4, H_2/CO_2, and CO_2/H_2 separations. Figure 2 (a) shows the CO_2/N_2 upper bound with the strongest temperature dependence, which is in line with the assumption that the separation mainly arises from the solubility selectivity (see Table 1). In order to enhance the selectivity, most CO_2/N_2 separation membranes are operated at 25–35°C [54]; some polyimide membranes are even operated at sub-ambient conditions in order to gain the selectivity [55-57].

Similarly, the CO_2/CH_4 upper bound depicted in Figure 2 (b) shifts downwards with increasing temperature since the separation is driven by both the higher solubility and diffusivity of CO_2 relative to CH_4. However, the temperature dependence is less pronounced compared with the CO_2/N_2 upper bound due to the smaller difference in the condensability values between CO_2 and CH_4.

For H_2/CO_2 separation illustrated in Figure 2 (c), the upper bound shifts upwards with increasing temperature due to the strong decrease in the CO_2 solubility at a higher temperature. This feature is the basis of using H_2-selective membranes in high-temperature applications such as syngas purification [6]. A particular scenario is the CO_2/H_2 separation demonstrated in Figure 2 (d), where a reverse-selective membrane must be used to separate the slow-diffusing but more condensable species [58]. In this case, a lower temperature again is beneficial for the separation because of the enhanced solubility selectivity.

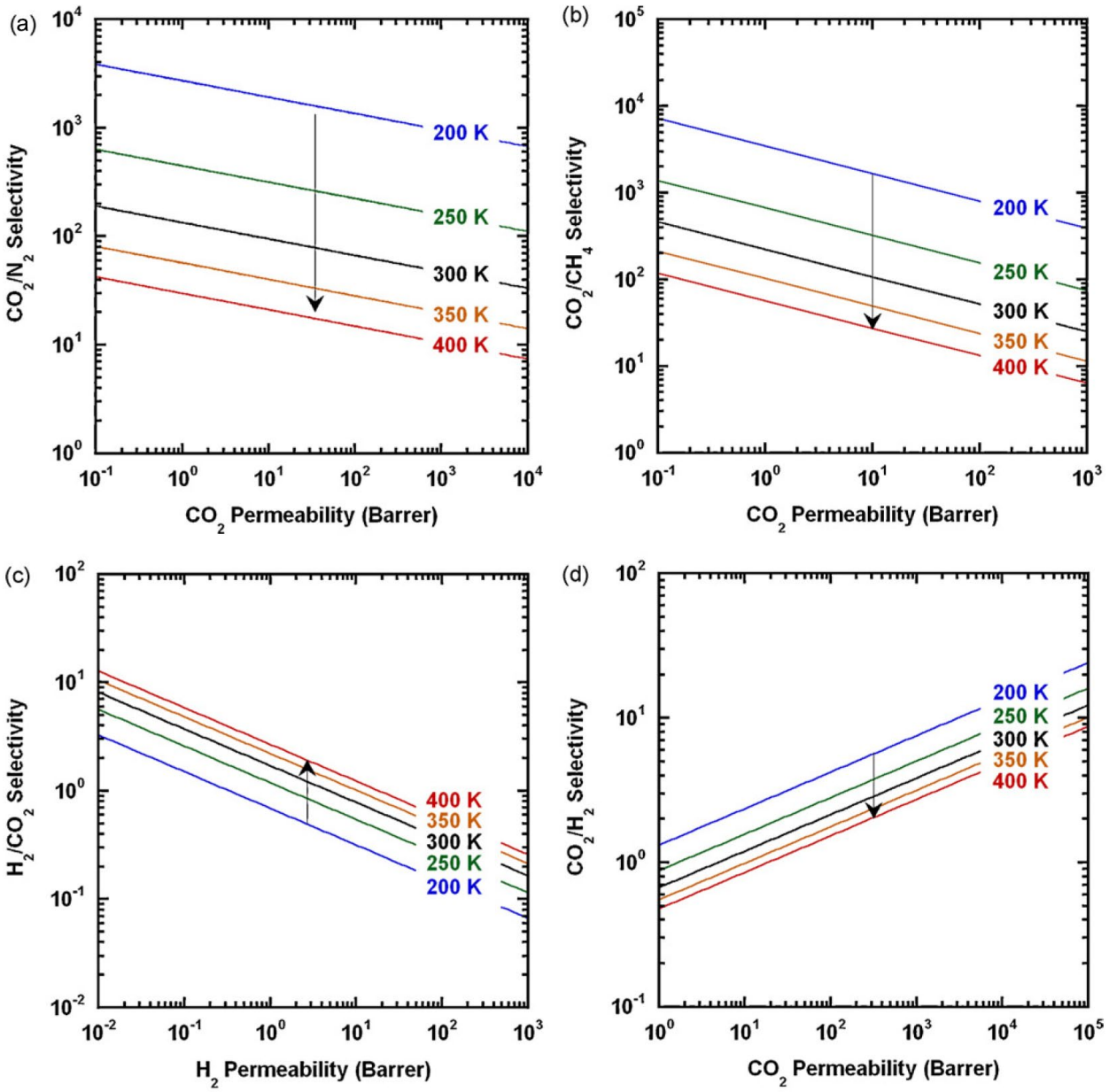

Figure 2. Effects of temperature on the predicted upper bounds for (a) CO_2/N_2, (b) CO_2/CH_4, (c) H_2/CO_2, and (d) CO_2/H_2. Adapted from Ref. [53]; copyright Elsevier.

Other noteworthy theoretical work to ascertain the upper bound behavior includes the group contribution methods developed by Park and Paul [59] and by Robeson et al. [60], respectively, for the prediction of permeability and selectivity of aromatic polymers, and the data-driven method

developed by Alentiev and Yampolskii [61]. Other theories have also been employed to interpret the upper bound behavior, such as the lattice fluid theory for the solubility upper bound [62], the cohesion energy density theory for the diffusivity upper bound [63], the free volume theory for the permeability upper bound in a highly plasticizing environment [64,65], and the resistance-in-series model for the permeance upper bound for thin-film composite (TFC) membranes [66]. The improved understanding of the permeability/selectivity trade-off not only defines the boundary of membrane technology in CO_2 separation and capture, but also points out the potential and direction for polymer and membrane research.

2.3. Facilitated transport mechanism

As indicated by Eq. (11), the value of β_{ij} is constrained by the S_i/S_j term, which is entirely determined by the Lennard-Jones temperatures of the gas pair (see Eq. (4)). Since the location of the upper bound is mainly controlled by β_{ij}, the permeability/selectivity trade-off is intrinsically caused by the limited physical solubility selectivity. One approach to overcome the upper bound limit is to introduce reactive moieties that can reversibly react with CO_2 in a polymeric membrane [67]. The reactive moiety is often termed as a carrier, and membranes containing carriers are typically referred as facilitated transport membranes (FTMs).

In a CO_2-selective FTM, CO_2 molecules dissolve in the polymer on the high-pressure side and react with the carriers to form reaction products. Because of the reversibility of the CO_2–carrier reaction, the dissolution includes both the physisorption and chemisorption of CO_2. Provided certain mobility, the reaction products diffuse down the concentration gradient across the membrane. On the low-pressure side, the low CO_2 partial pressure leads to the dissociation of the reaction products, by which the CO_2 molecules are released and the carriers are regenerated. The

reactive diffusion scheme does not exclude the solution-diffusion of unreacted CO_2 molecules. Similar to the dual mode sorption model in glassy polymers [43], the overall CO_2 flux through a FTM can be expressed as:

$$J_{CO_2} = \frac{P_{CO_2}}{\ell}\Delta p_{CO_2} + \frac{P_{\text{carrier-}CO_2}}{\ell}\Delta p_{\text{carrier-}CO_2} \quad (12)$$

where the first term on the right-hand side is the contribution from the solution-diffusion of CO_2, while the second term represents the facilitated transport [68,69]. The reactive diffusion enhances the transport of CO_2. On the contrary, other inert gases (e.g., H_2, N_2, and CH_4) cannot react with the carriers and their fluxes based on the solution-diffusion mechanism are typically a few orders of magnitude lower than that of CO_2 [26].

Amines are the most exploited carriers for the synthesis of CO_2-selective FTMs owing to the rich amine–CO_2 chemistry. CO_2 can react with a primary or secondary amine as a electrophile and form a zwitterion [70]:

$$CO_2 + R\text{–}NH_2 \rightleftharpoons R\text{–}NH_2^+\text{–}COO^-$$

The zwitterion quickly degenerates to a carbamic acid via an intramolecular proton transfer:

$$R\text{–}NH_2^+\text{–}COO^- \rightleftharpoons R\text{–}NH\text{–}COOH$$

The carbamic acid then reacts with another amine to form carbamate and ammonium ions:

$$R\text{–}NH\text{–}COOH + R\text{–}NH_2 \rightleftharpoons R\text{–}NH\text{–}COO^- + R\text{–}NH_3^+$$

This so-called "zwitterion mechanism" requires 2 moles of primary or secondary amine for 1 mole of CO_2.

A tertiary amine, on the other hand, cannot form carbamate with CO_2 because of the lack of a labile proton. Instead, it reacts with CO_2 following a Brønsted acid-base reaction in the presence of water:

$$CO_2 + R_1R_2\text{–}N\text{–}R_3 + H_2O \rightleftharpoons HCO_3^- + R_1R_2\text{–}NH^+\text{–}R_3$$

where 1 mole of tertiary amine is needed for 1 mole of CO_2. Although tertiary amines exhibit an advantageous reaction stoichiometry relative to primary and secondary amines, their reaction kinetics is severely limited by the slow formation rate of carbonic acid from CO_2 and water [71].

Figure 3 shows a schematic of CO_2 transport vs. other inert gases through an amine-containing FTM [72]. As seen, the carrier can either be polymeric with amino groups covalently bound to the polymer backbone, or a small molecular amine that is mobile in the polymer matrix. The former is often termed as a fixed-site carrier while the latter as a mobile carrier [73]. For the fixed-site carrier, the amino groups can only fluctuate near their equilibrium positions. In this case, CO_2 molecules can hop among neighboring amino groups via the formation and breakage of the carbamate bond [72-75]. The mobile carrier, on the other hand, can form a mobile carbamate or bicarbonate ion with CO_2, which typically possesses a better mobility compared with the hopping mechanism for the fixed-site carrier [76].

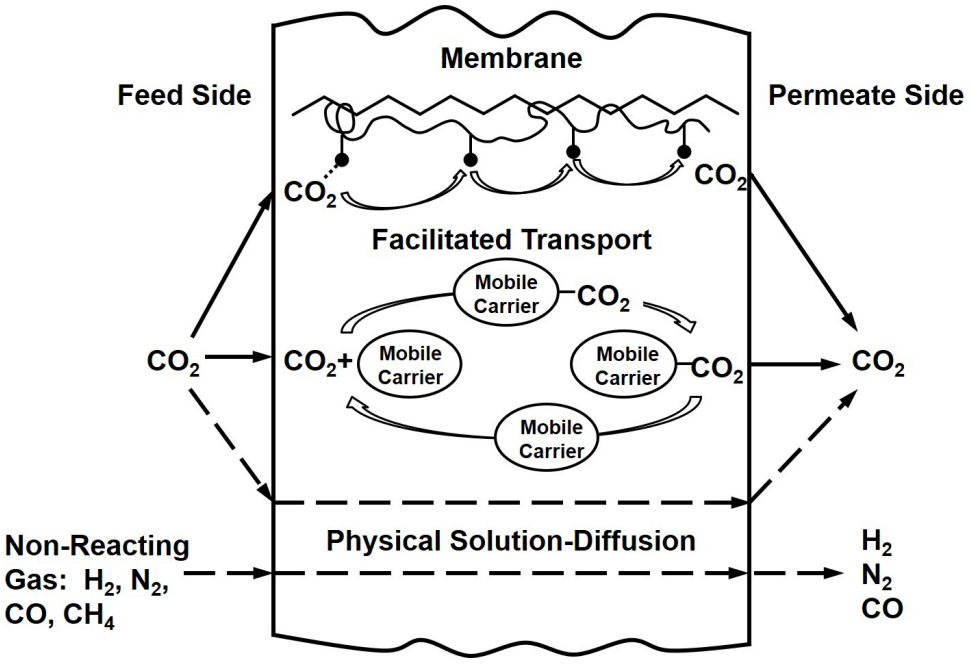

Figure 3. Schematic of gas permeation through a facilitated transport membrane. Adapted from Ref. [77]; copyright American Chemical Society (ACS).

3. Emerging Polymeric Membrane Materials

Emerging polymeric membrane materials for CO_2/gas separation are reviewed in this section based on the polymer architecture and the polymer–CO_2 interaction. Seven classes of polymers are discussed, including (1) ether oxygen-rich polymers, (2) polymeric ionic liquids, (3) perfluoropolymers, (4) thermally rearranged polymers, (5) glassy polymers with iptycene as building block, (6) other non-reactive polymers, and (7) facilitated transport polymer membranes. Other important membrane families such as mixed matrix membranes and carbon molecular sieve membranes are beyond the scope of this review, but their information can be found in recent reviews [78,79].

3.1. Ether oxygen-rich polymers

Among the many efforts to enhance the CO_2 solubility selectivity in polymers, the most successful example is a family of rubbery polymers that contain high content of ether oxygen [80-82]. It is known that CO_2 is affinitive to ether (–C–O–C–) linkage via quadrupole-quadrupole interaction [83]. Due to the uneven distribution of charges in the ether linkage, the carbon atoms carry partially positive charge while the oxygen atom is partially negative. The symmetric CO_2 molecule has a permanent electrical quadrupole moment and tends to align its oxygen atoms near the positively charged regions (carbon) of the ether-containing polymer while positioning its carbon atom near the negatively charged regions (oxygen). This net attraction promotes the solvation of CO_2 and the CO_2 solubility could increase with a greater content of ether oxygen.

Liu et al. used density functional theory (DFT) and studied the binding geometries between CO_2 and three oligomers: nonane (O:C = 0), diethylene glycol dimethyl ether (diglyme) (O:C = 0.5), and 1-methoxy-2-(methoxymethoxy)ethane (TOO) (O:C = 0.6) [84]. As shown in Figure 4, a higher O:C ratio increases the binding energy and potentially could enhance the CO_2 solubility.

Albeit its high affinity to CO_2, flexible ether linkages tend to form semi-crystalline regions in polymers. For instance, poly(ethylene oxide) (PEO) has a O:C ratio of 0.5 but a low CO_2 permeability of merely 12 Barrer [85]. These semi-crystalline regions not only hamper the diffusion of CO_2, but also make the ether groups inaccessible to CO_2 interaction.

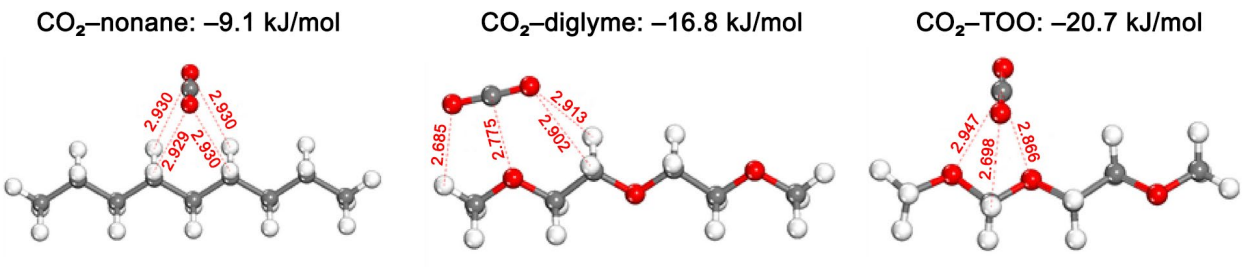

Figure 4. Binding geometries and energies of CO_2 and oligomers with various ether oxygen contents. Bond lengths are in the unit of Å. Key: C, gray; O, red; H, white. Adapted from Ref. [84]; copyright Elsevier.

In order to suppress the crystallinity of ether oxygen-rich polymers, various approaches have been developed in the literature, including (1) copolymerization with bulky, rigid segment, (2) blending with low MW moiety to disrupt chain packing, and (3) formation of secondary polymer chains by crosslinking or branching. The CO_2 permeabilities and CO_2/gas selectivities of representative emerging ether oxygen-rich polymers are summarized in Table S1 in the Supporting Information (SI) based on the synthesis strategy.

Block-copolymerization of ethylene oxide segments and certain rigid segments is an efficient method to suppress the crystallinity of PEO. The hard segments disrupt the chain packing and increase the fractional free volume (FFV), while the soft ethylene oxide segments are responsible for the CO_2 affinity. The first few ether-rich block copolymers are under the trade name Pebax®

and Polyactive™, in which polyamide (PA) and poly(butylene terephthalate) (PBT) are used as the rigid segments, respectively [37,86]. Compared with PEO, these commercial copolymers exhibited an improved CO_2 permeability as high as 150 Barrer with a CO_2/N_2 selectivity ca. 50 at 25°C. Particularly, the CO_2/N_2 selectivity is of interest for CO_2 capture from dilute sources such as flue gases [16]. TFC membranes were synthesized with these block copolymers [87], and a high CO_2 permeance of 1815 GPU with a CO_2/N_2 selectivity of 50 was reported by Yave et al. [88].

Other even bulkier rigid segments have also been used and reported in the literature, such as polyvinyl chloride (PVC) [89], polyacrylonitrile (PAN) [90,91], and pentiptycene-based polyimide (Pent-PI) [92,93]. Reijerkerk et al. synthesized a block copolymer based on a poly(ethylene oxide-*ran*-propylene oxide) (PEO-*ran*-PPO) soft segment and a monodisperse tetra-amide (T6T6T) hard segment [55]. This copolymer exhibited a high CO_2 permeability of 470 Barrer and a CO_2/N_2 selectivity of 43 at 35°C.

In order to refrain the crystallinity in the abovementioned block copolymers, the fraction of the ethylene oxide phase typically is low, which limits the solubility of CO_2. Therefore, the block copolymers are often blended with ether-containing oligomers to enhance the membrane performance. Short chain polyethylene glycol (PEG) with a MW of 100–2000 Da was blended with Polyactive™ [86] and Pebax® [94], and the increased ether content rendered a CO_2 permeability greater than 500 Barrer with a CO_2/N_2 selectivity higher than 30. The improved CO_2 permeability was attributed to the higher CO_2 solubility as well as the higher free volume.

The terminal groups on PEG could also provide another control to disrupt the packing of the ethylene oxide phase. Yave et al. blended PEG-dibutyl ether (PEG-DBE) with Polyactive™ and registered a high CO_2 permeability of 750 Barrer with a CO_2/N_2 selectivity of 40 at 30°C [86].

PEG moieties with terminal groups, such as methyl ether, ally ether, divinyl ether, butyl ether, etc., were incorporated into Pebax® MH1657 [95]. In general, these terminal substituents eliminated the hydrogen bond donors on PEG, making the polymer blends more permeable to CO_2.

Other ether-containing brush polymers have also been used to further increase the free volume of the polymer blends. Reijerkerk et al. used poly(dimethylsiloxane-*co*-methyl(3-hydroxypropyl)siloxane)-*g*-poly(ethylene glycol)methyl ether (PDMS-*g*-PEGME) as the ether additive, resulting in a CO_2 permeability of 896 Barrer with a CO_2/N_2 selectivity of 36 at 35°C [96]. A self-crosslinkable poly(glycidyl methacrylate-*g*-polypropylene glycol)-*co*-poly(oxyethylene methacrylate) (PGP-POEM) brush polymer was added in Pebax-1657, which led to a 2.5-fold enhancement in CO_2 permeability compared to the neat membrane [97]. TFC membranes were also synthesized by blending poly(ethylene glycol)dimethyl ether (PEGDME-500) [98] and poly(ethylene glycol)-*b*-poly(pentafluoropropylacrylate) (PPFPA) [99] into Pebax®. These TFC membranes demonstrated a CO_2 permeance of 940 GPU with a surprisingly high CO_2/N_2 selectivity of 30 at an elevated temperature of 57°C.

Ether-rich polymers can also be synthesized via the crosslinking of ethylene oxide-containing monomers or oligomers. The initial work was based on the photopolymerization of various methacrylate monomers, where chain packing was an impossibility in the highly crosslinked polymer network [100-105]. Another interesting building block for the crosslinked ether-rich network is polyether terminated with amino groups. Jeffamine®, a commercial polyether diamine, has been used to crosslink with multidentate epoxide [106-108] and acyl chloride [109]. A recent work by Li et al. demonstrated the crosslinking of diethylene glycol bis(3-aminopropyl)ether (DGBAmE) and trimesoyl chloride (TMC) via interfacial polymerization; the TFC membrane exhibited a CO_2 permeance of 1310 GPU with a CO_2/N_2 selectivity of 33 at 22°C [110].

Recently, a new family of comb polymers have been synthesized by Liu et al. using heterocyclic acetals [84]. Alkoxy acrylate was used to induce the ring opening of the heterocyclic acetal and subsequently graft the ether-containing segment onto the vinyl substrate. This vinyl monomer was then photopolymerized to afford a vinyl polymer with side chains containing ether groups. As shown in Figure 5, a poly(1,3-dioxolane) with a high O:C ratio of 0.67 exhibited a high CO_2 permeability of 1400 Barrer and a CO_2/N_2 selectivity of 64 at 70°C. This might be the first polyether that demonstrated a high CO_2/N_2 selectivity at a temperature considerably higher than room temperature. Liu and coworkers also used 1,3,5-trioxane as the cyclic acetal and achieved an O:C ratio of 0.8 in the synthesized comb polymer [111]. However, this polymer possessed a low FFV due to the extremely high ether content, thus a low CO_2 permeability.

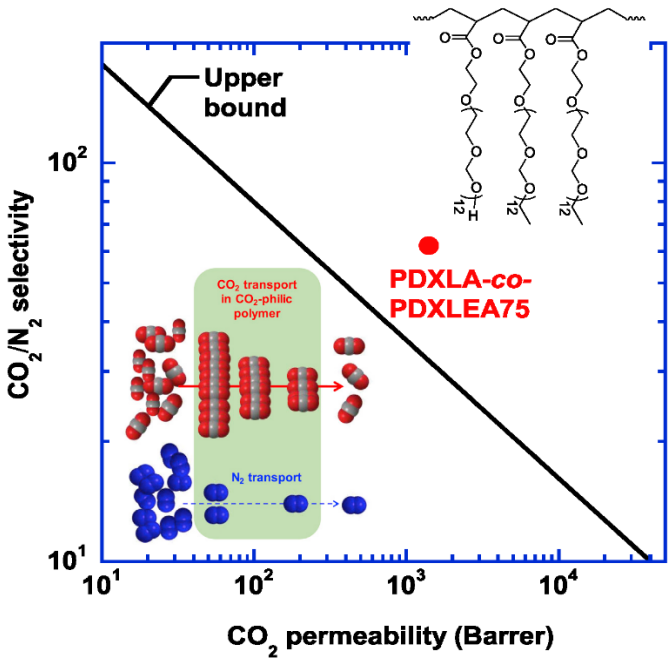

Figure 5. Structure and CO_2/N_2 transport performance of poly(1,3-dioxolane) at 70°C. Adapted from Ref. [84]; copyright Elsevier.

Despite the great potential of the ether-rich polymers for CO_2/N_2 separation, these polymers do not possess sufficient CO_2/H_2 and CO_2/CH_4 selectivities for applications such as pre-combustion carbon capture and natural gas sweetening (see Table S1 in the SI). As discussed in Section 2.1, the low CO_2/H_2 diffusivity selectivity offsets the benefit of the high CO_2/H_2 solubility selectivity contributed by the ether groups. These polymers also lack the size-sieving ability to enhance the CO_2/CH_4 diffusivity selectivity. A recent work by Harrigan et al. used methylidynetri-*p*-phenylene triisocyanate (PTI), a tridentate rigid crosslinker, to polymerize PEG oligomers [112]. The rigidification of the crosslinked PEG provided certain hindrance on the diffusion of CH_4, which rendered a CO_2/CH_4 selectivity greater than 60 but a low CO_2 permeability of 0.07 Barrer.

3.2. Polymeric ionic liquids

Room temperature ionic liquids (RTILs) are organic/inorganic salts that exhibit liquid-like properties at ambient conditions. RTILs are typically non-volatile and thermally stable owing to the strong ionic strength. RTILs have been widely studied as absorbents for CO_2 capture due to their high CO_2 solubility and low volatility [113]. In addition, supported liquid membranes (SLMs) have been synthesized by impregnating RTILs into porous membranes [114-117]. These SLMs showed potentials for CO_2/N_2 and CO_2/CH_4 separations, but cannot withstand a high transmembrane pressure differential, under which the RTILs tend to leach out [114]. The stability concerns sparked the development of polymeric ionic liquids (poly(RTIL)s) [118,119]. Based on how the IL moieties are incorporated in the polymer, the poly(RTIL)s can be categorized into three motifs: (1) crosslinked ion-gel membranes, (2) poly(ionene)s, and (3) poly(ionomer)s. The CO_2 vs. gas transport performances of relevant poly(RTIL)s are summarized in Table S2 in the SI based on the synthesis strategy.

A natural extension of the SLM concept is to use a highly crosslinked polymer rather than a porous membrane to host the RTILs. The RTIL is often blended with the monomer or oligomer prior to the crosslinking so that a molecularly mixed ion-gel mixture can be formed. Various crosslinked polyethers have been synthesized as the hosting polymers. On one hand, a high content of RTILs can be impregnated into proper polyethers without phase separation; on the other hand, the RTILs can plasticize these polyethers and significantly enhance the gas diffusivity [120]. The most common synthesis scheme is to photopolymerize an ethoxylated acrylate monomer with a multi-amine via Michael addition [121] or with a multi-thiol via thiol-Michael addition [122]. At least one of the two monomers should be tridentate in order to form the crosslinked network.

In a recent work by Deng et al., poly(ethylene glycol) diacrylate (PEGDA) was polymerized with a triamine, tris(2-aminoethyl)amine (TAEA) to form an ether-rich rubber as shown in Figure 6 with a glass transition temperature below –40°C [121]. Four conventional RTILs with different anions (i.e., [Bmim][BF_4], [Bmim][PF_6], [Bmim][TCM], and [Bmim][Tf_2N]) were blended with the polymer network at a RTIL loading as high as 80%. Among them, the membrane containing [Bmim][Tf_2N] demonstrated the best CO_2 permeability of 135 Barrer and a CO_2/N_2 selectivity of 45 at 35°C.

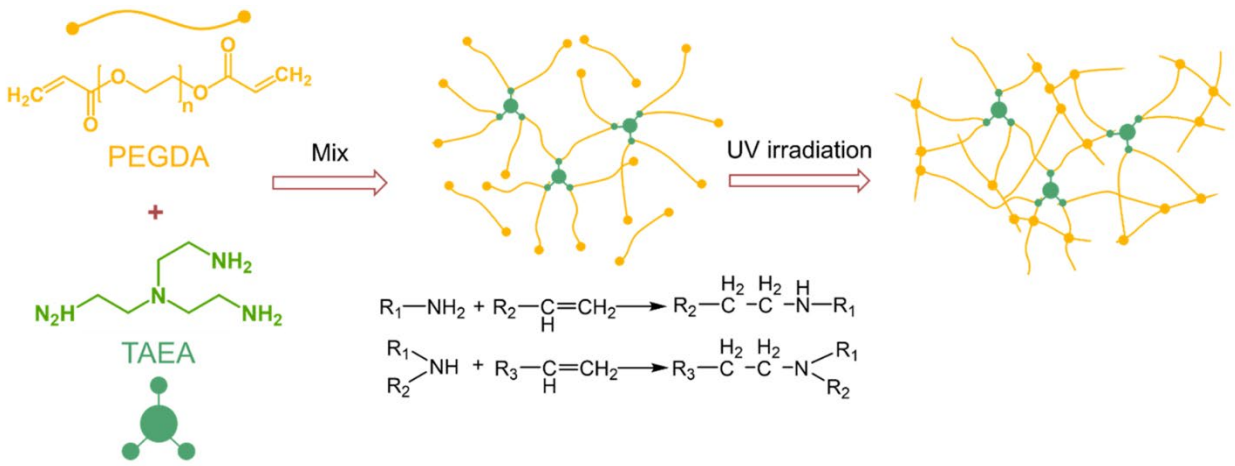

Figure 6. Synthesis scheme of the cross-linked tris(2-aminoethyl)amine-poly(ethylene glycol) diacrylate membrane. Adapted from Ref. [121]; copyright ACS.

A polymer network with an even higher ether oxygen content was reported by Kusuma et al. by using 3,6-dioxa-1,8-octanethiol and ethoxylated trimethylolpropane triacrylate, a branched acrylate with a 20:3 ethylene glycol/acrylate ratio [122]. The cation effect of the RTIL was studied by incorporating a series of [Tf_2N]-based RTILs into the ion-gel membranes, with [emim][Tf_2N] showing the highest CO_2 permeability of 529 Barrer and a CO_2/N_2 selectivity of 31 at 40°C. In this case, the imidazolium ring in the $[emim]^+$ cation was closely associated to the ether linkage through the acidic proton on the C-2 position of the imidazolium ring, leaving the two terminal methyl groups dangling away from the polymer chain [123]. This short chain impingement further plasticized the polymer network (evidenced by a reduced glass transition temperature from –44 to –61 °C), leading to a higher gas diffusivity.

The PEG-based thiol could also be replaced by a thiol-decorated polysiloxane, and the resultant PEO-siloxane copolymer improved the CO_2/N_2 selectivity to 54 at 40°C [124]. It is apparent that subtle changes to the polymer structure could greatly affect the gas permeability and selectivity. In general, an ethoxylated acrylate with a shorter PEG chain often results in a tighter polymer

network, which tends to (1) limit the impregnation of a high content of RTILs, (2) render a lower free volume of the ion gel, and (3) result in a more fragile film [120].

The high CO_2/N_2 separation performance of the abovementioned ion-gel membranes is only achievable at a high RTIL content. However, phase separation can occur with increasing RTIL loading, and the phase stability generally weakens at a higher temperature [125,126]. In order to address these membrane formation issues, methods to incorporate the ionic groups directly onto the polymer have been developed, and these research efforts follow two motifs: poly(ionene)s and poly(ionomer)s. In a poly(ionene), a cationic or anionic group is directly constructed in the polymer backbone; however, the ionic group is connected to the polymer chain as a pendent group in a poly(ionomer).

A series of rigid poly(ionene)s were synthesized by Bara's group by incorporating imidazolium group into Tröger's base-containing polymers [127] and polyimides [128] with $[Tf_2N]^-$ as the counterion. These poly(ionene)s did not exhibit any nanoscale phase separation, but the rigid polymer backbone resulted in a low free volume and thus a low CO_2 permeability less than 20 Barrer. A more successful effort was reported by Yin et al. for the synthesis of a new imidazolium monomer with two amino terminal groups [129]. As shown in Figure 7, this monomer was polymerized with diglycidyl ether and triglycidyl ether, resulting in linear and branched poly(ionene)s, respectively. After blending with [emim][Tf_2N], the branched poly(ionene) showed an exceptional CO_2 permeability of 2070 Barrer and a decent CO_2/N_2 selectivity of 25 at 35°C.

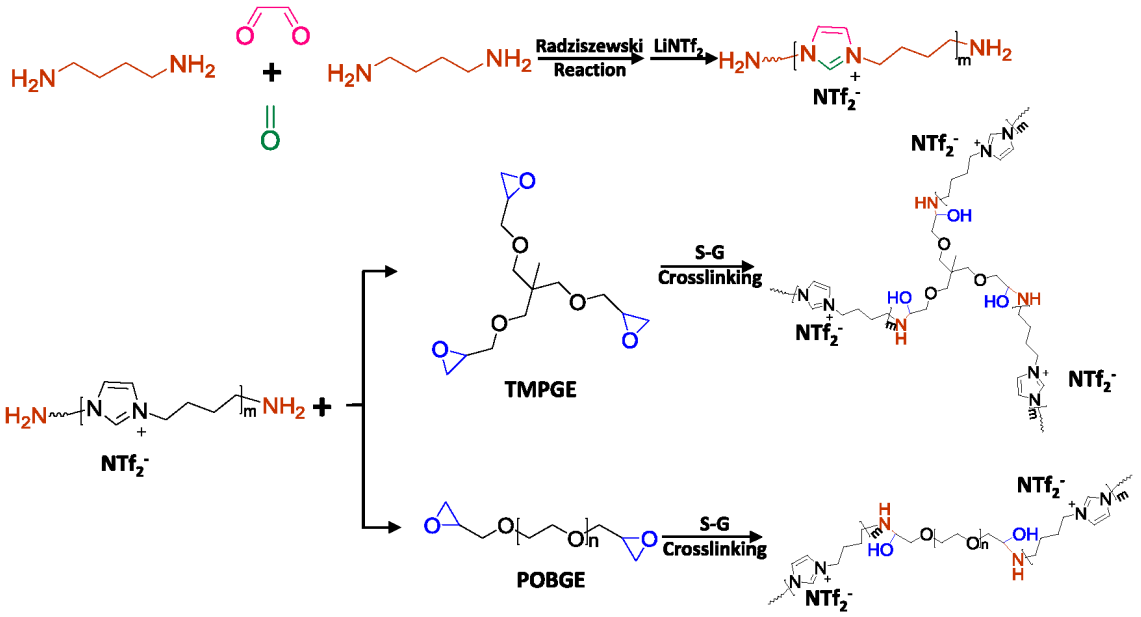

Figure 7. Synthesis of crosslinked poly(ionene) via the Debus-Radziszewski reaction. Adapted from Ref. [129]; copyright Elsevier.

Compared with the poly(ionene)s, poly(ionomer)s are typically low-free-volume glassy polymers with unattractive gas separation performance themselves. However, low MW RTILs can serve as permanent plasticizers and greatly enhance the polymer free volume. Ito et al. incorporated 1-butyl-3-methylimidazolium bis(trifluoromethane)sulfonimide ([C_4mim][Tf_2N]) into a sulfonated polyimide [130]. At a loading of 75 wt.% of the RTIL, a bicontinuous nanostructure was formed with IL-rich and IL-lean phases, resulting in a high modulus of the film and a CO_2 permeability of 431 Barrer with a CO_2/N_2 selectivity of 30 at 30°C. Once again, a softer polymer chain generally improves the gas diffusivity in the poly(ionomer).

Linear pyrrolidinium polycation ($[HPyr]^+$) has been reported to yield a higher CO_2 diffusivity than other rigid poly(ionomer)s [131]. The membrane performance was greatly improved when this poly(ionomer) was paired with bulky cyano-functionalized anions, such as $[C(CN)_3]^-$,

$[N(CN)_2]^-$, and $[B(CN)_4]^-$ [131,132]. These bulky anions outperformed the conventional $[Tf_2N]^-$ anion and demonstrated a CO_2/N_2 selectivity as high as 61 at 20°C.

Similar to the ether oxygen-rich polymers, poly(RTIL) membranes lack the size-sieving ability and mainly rely on the CO_2/gas solubility selectivity for the separation. Therefore, most of the work in this area targeted CO_2/N_2 separation. CO_2/CH_4 separation data were occasionally reported [127,128] while application in CO_2/H_2 separation is seldomly seen.

3.3. Perfluoropolymers

Perfluoropolymers are a family of fluorinated polymers with most or all the C–H bonds replaced by stronger C–F bonds. The high C–F bond energy (485 kJ/mol vs. 346 kJ/mol for C–C bond) and the protective sheath of the bulky fluorine atoms around the C–C polymer backbone make perfluoropolymers extremely resistant to harsh thermal and chemical environments [133]. Although the early generations of fluorinated vinyl polymers (e.g., polytetrafluoroethylene (PTFE)) were extensively used in numerous commercial applications, they did attract much interest in gas separation due to the low gas permeability and poor solvent processability [134].

However, since mid-1980s, a new class of amorphous perfluoropolymers were developed, such as Teflon™ AF, Hyflon™ AD, and Cytop™ as shown in Figure 8. The bulky dioxole monomer disrupts the chain packing, which renders a higher gas diffusivity as well as a better solubility in fluorinated solvents [135]. The CO_2/gas separation performances of these commercial perfluoropolymers are summarized in Table S3 in the SI. As seen, these amorphous glasses generally exhibited a high CO_2 permeability, which was partly attributed to the pre-existing microchannels in these materials [136]. For instance, Teflon™ AF2400 showed a CO_2 permeability as high as 2200 Barrer at 35°C [137]. Various fluorocarbon solvents, e.g., Vertrel®

XF and Novec™ 7200, have been developed and allowed for the solvent processing of these perfluoropolymers into TFC membranes, which demonstrated a CO_2 permeance greater than 1000 GPU [138]. A pitfall of these commercial perfluoropolymers, however, is the low CO_2/gas selectivity. Although certain CO_2/CH_4 separation could be observed due to the overall low hydrocarbon sorption (e.g., CH_4), the permselectivity is inadequate for applications such as natural gas sweetening [139].

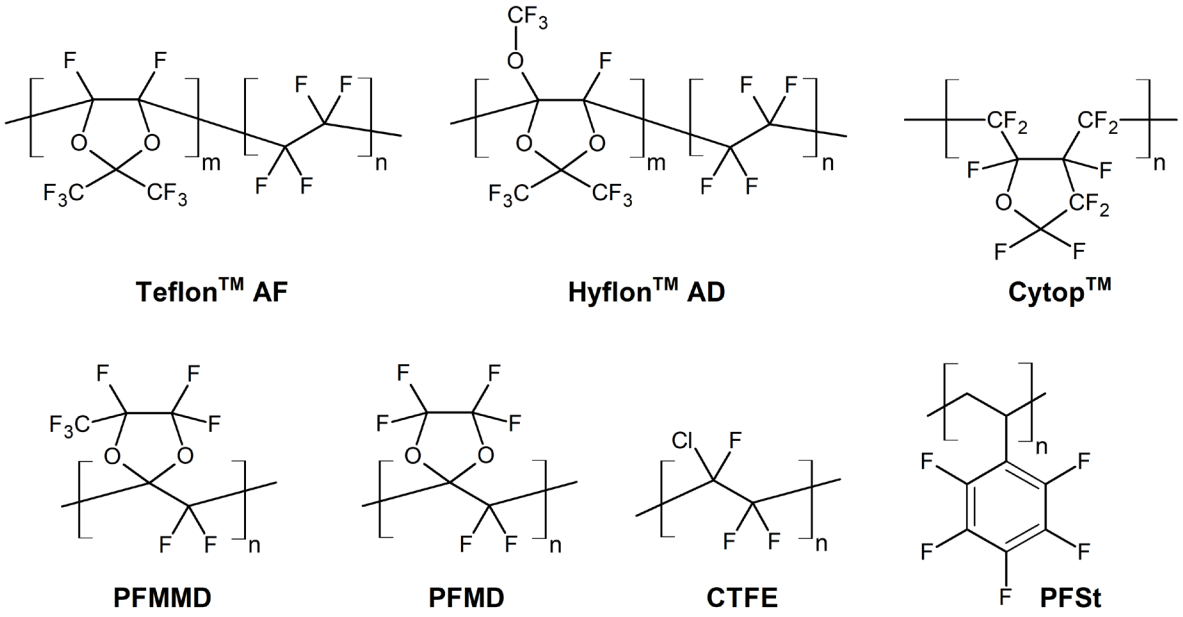

Figure 8. Structures of commercial fluorinated polymers and perfluorodioxolane polymers.

A noticeable trend of research in this area is the synthesis of novel perfluorodioxolane monomers such as perfluoro-(2-methylene-4-methyl-1,3-dioxolane) (PFMMD) and perfluoro-(2-methylene-1,3-dioxolane) (PFMD). Although the homopolymers of these perfluorodioxolane monomers (see Figure 8) did not show promising CO_2/gas separation performance [140], these monomers can be copolymerized with other existing fluorovinyl monomers. For instance, Belov

et al. copolymerized PFMMD with pentafluorostyrene (PFSt), resulting a copolymer that was soluble in common solvents such as acetone and tetrahydrofuran [141].

A more versatile synthesis route was developed by Fang et al., where PFMMD was copolymerized with PFMD and chlorotrifluoroethylene (CTFE), respectively [142]. Although these copolymers were only soluble in specialty fluorinated solvents, TFC membranes were synthesized with a selective layer thickness of ca. 200 nm, and the membranes demonstrated a CO_2 permeance greater than 400 GPU and a high CO_2/CH_4 selectivity of 55. An alternative approach is to add perfluoropolyether into the perfluorodioxolane as a plasticizer. Chiang et al. reported that the addition of Fomblin® Z60 ($(–CF_2–CF_2–O–)_n$, n = 112) in poly(PFMMD) greatly increased the CO_2 permeability with a slight reduction in the CO_2/CH_4 selectivity [143].

The physical aging and plasticization by hydrocarbon vapors have also been studied for commercial perfluoropolymers [144-147]. Perfluoropolymers showed a slower physical aging compared with other high-free-volume glassy polymers. In addition, the low hydrocarbon sorption also bestowed perfluoropolymers the ability to retain the CO_2/CH_4 selectivity under highly plasticizing conditions. Therefore, novel amorphous perfluoropolymers can be well-suited for natural gas sweetening.

3.4. Thermally rearranged (TR) polymers

In 2007, Park et al. reported a new class of polymers where rigid and planar macromolecules could be formed by the thermal rearrangement of polyimides and polyamides containing *ortho*-functionalized groups [148]. The general scheme of the thermal rearrangement is shown in Figure 9. For a poly(hydroxyimide) precursor (i.e., TR-α precursor), an intramolecular cyclization is initiated between the hydroxyl and imide groups with a quantitative loss of CO_2. The TR process

leads to the formation of a rigid rod-like benzoxazole-phenylene structure (TR-α-PBO), which disrupts the chain packing and renders a bimodal cavity distribution [148-151]. The larger cavities serve as the channels for fast gas diffusion, while the smaller ones are capable of molecular sieving [152].

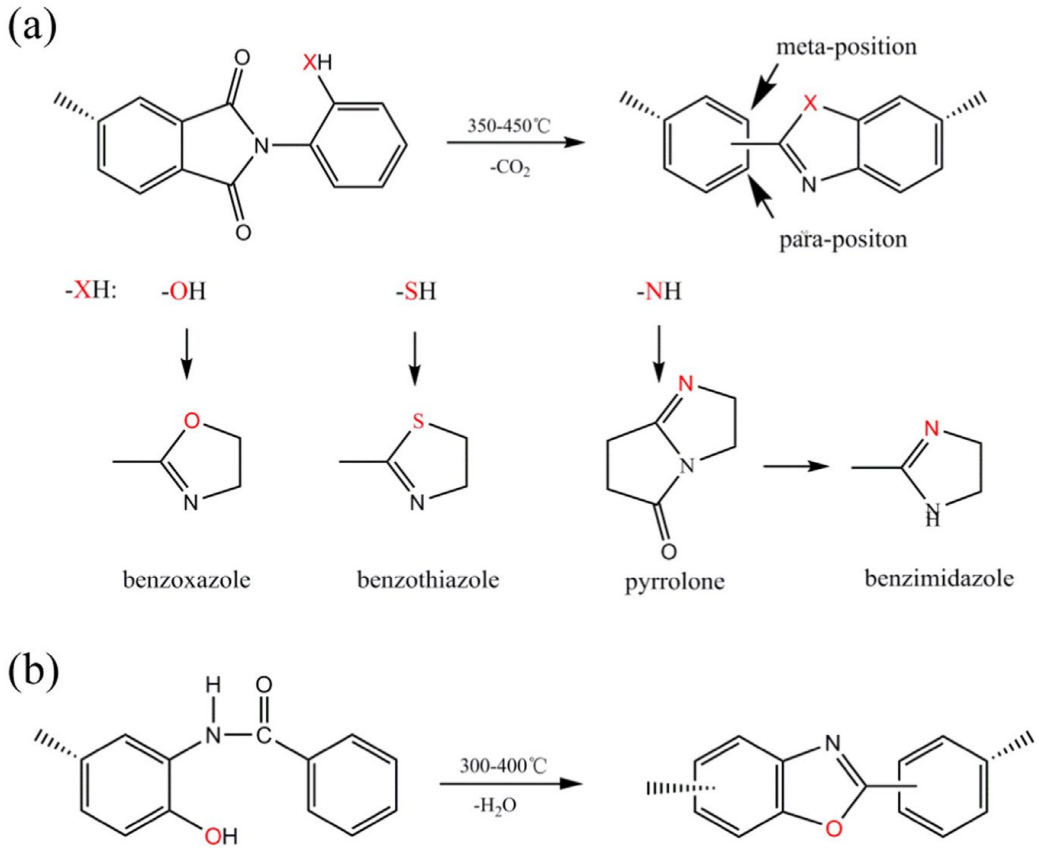

Figure 9. Thermally rearrangement mechanism of (a) TR-α and (b) TR-β. Adapted from Ref. [153]; copyright Elsevier.

Similar TR processes can occur for amino group in the ortho position, resulting in the formation of polybenzimidazole (PBI) (TR-α-PBI) [154]. The TR reaction for thiol group has also been proposed as shown in Figure 9 (a), but to the best of our knowledge, no example of the resultant TR polybenzothiazole has been reported in the literature, likely due to the poor nucleophilicity of the thiol group [155].

Table S4 in the SI summarizes the transport properties of several TR-α polymers as well other selected TR polymers. These TR-α polymers exhibited CO_2 permeabilities as high as 4045 Barrer with CO_2/N_2 selectivities higher than 20 and CO_2/CH_4 selectivities in the range of 40–50. Positron annihilation lifetime spectroscopy and molecular modeling have shown that the conversion of the polyimide precursor to the TR-α-PBO or TR-α-PBI led to an increase in the free volume, thereby increases in both gas diffusivity and solubility [156-158]. Hollow-fiber (HF) membranes were also prepared by TR-α-PBO with a high CO_2 permeance of 2500 GPU and a CO_2/CH_4 selectivity of 22 [159,160].

In order to produce TR-α polymers with good separation performance, the polyimide precursors are generally treated at >400°C, and the resultant films are often brittle and cannot be made into a modular configuration [161]. One approach to reduce the TR temperature is to use *ortho*-functionalized poly(hydroxyamide)s as the precursors as shown in Figure 9 (b). TR polymers synthesized following this route are termed as TR-β polymers. The synthesis of the polyamide precursor involves the use of a diacyl chloride rather than the bulkier dianhydride used for TR-α polymers. In addition, the aromatic amide linkage is more flexible than the aromatic imide linkage for the same hydroxyl group at the ortho position. As a result of these two factors, the TR temperatures into TR-β polymers are about 100°C lower than those for TR-α polymers, but the cavity size of TR-β polymers is also smaller [153,162,163]. Consequently, TR-β polymers generally exhibited lower CO_2 permeabilities as shown in Table S4 in the SI.

TR polymers are subject to physical aging like other glassy polymers with high excess free volume [164]. As shown in Figure 10 (a), chain relaxation caused the collapse of the microstructure of a TR-α-PBO, which led to a loss of CO_2 permeability but an increased CO_2/CH_4 selectivity [165]. However, the extent of aging was less severe compared with its

poly(hydroxyimide) precursor due to the overall higher chain rigidity. In-situ restoration was also demonstrated by exposing the TR polymers to methanol. As illustrated in Figure 10 (b), a TR-α-PBO HF went through the in-situ methanol treatment twice during a course of 703 days, and each time the CO_2 permanence was well recovered [166].

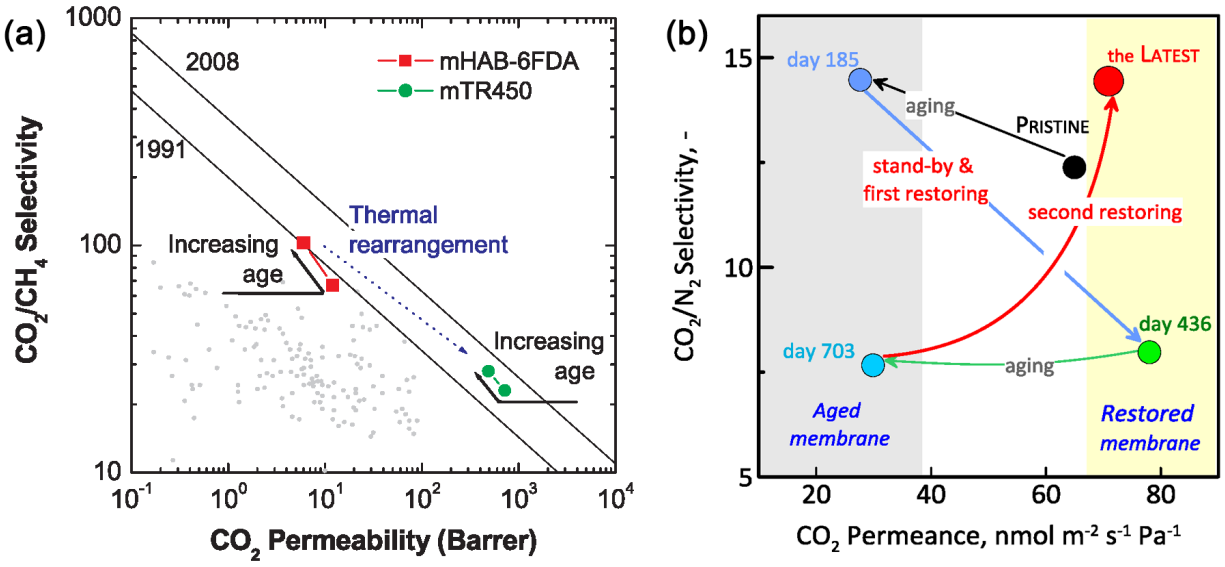

Figure 10. (a) Physical aging of a TR-α-PBO and its poly(hydroxyimide) precursor for 6 months; (b) Evolution of CO_2 permeance and CO_2/N_2 selectivity of a TR-α-PBO HF during physical aging and regeneration by methanol. Adapted from Refs. [165,166]; copyright Elsevier.

The brittleness and unsatisfactory membrane forming ability of TR-α polymers can also be addressed via crosslinking. Various attempts have been reported in the literature by using 3,5-diaminobenzoic acid (DABA) as a crosslinkable building block. DABA was used to synthesize the aromatic dianhydride and then polymerized with the hydroxy diamine to afford the crosslinkable poly(hydroxyimide) precursor. The carboxyl group on the DABA unit was then crosslinked by a mono-esterification reaction with diol [167] or by a decarboxylation reaction with

another DABA unit [168-170] as shown in Figure 11. Additional excess free volume was created during the crosslinking reaction, resulting in an improved CO_2 permeability. In addition, the interconnected polymer network can mitigate the plasticization of these glassy polymers in high-pressure applications such as natural gas sweetening.

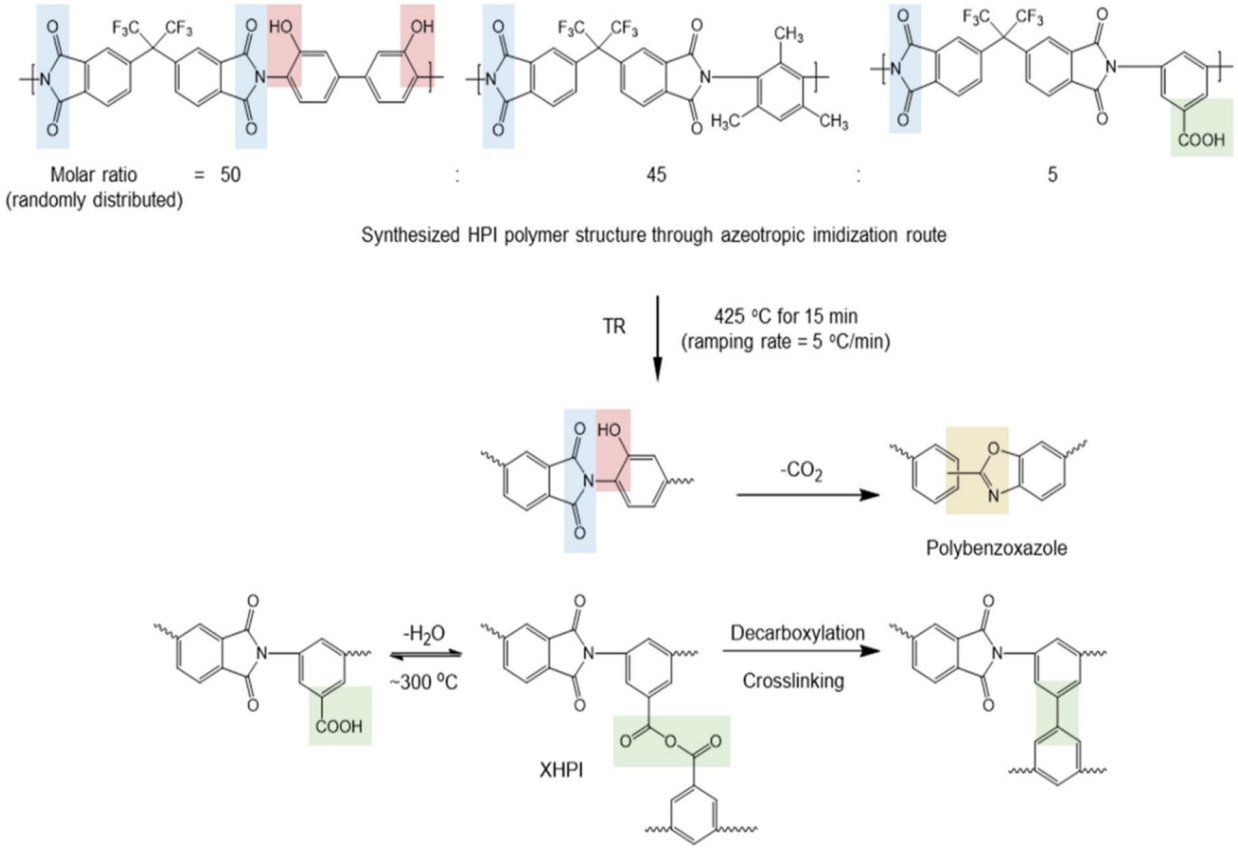

Figure 11. Schematic synthesis process of a crosslinked TR-α-PBO. Adapted from Ref. [170]; copyright Elsevier.

Copolymerization of TR polymers is another widely explored area with purposes of: (1) combining TR polymers with other glassy polymers such as aromatic polyamides [171] and polyimides [172] and (2) combining different TR polymers [173]. The incorporation of non-TR-

able glassy polymers could improve the mechanical properties of the TR polymers; the gas permeability changes based on the chain rigidity and bulkiness of the non-TR-able units. For instance, the incorporation of imide segments derived from 2,3,5,6-tetramethyl-1,4-phenylenediamine (4MPD) and 4,4′-(hexafluoroisopropylidene)diphthalic anhydride (6FDA) led to a reduced CO_2 permeability [172]; however, the CO_2 permeability was increased to a great deal when the diamine, 4MPD, was replaced by a bulky 9,9-bis(3-amino-4-hydroxyphenyl)fluorene (bisAHPF) unit [174].

A copolymer containing different types of TR units could exhibit advantageous characteristics from both TR polymers. For instance, Choi et al. synthesized a TR-PBO-*co*-PPL copolymer, which showed a good CO_2 permeability of 525 Barrer (from the TR-PBO units) and an exceptional CO_2/CH_4 selectivity of 78 (from the TR-PPL units) [173].

TR polymers can also be copolymerized with PIMs, another class of highly rigid polymer. The main characteristic of PIMs is their contorted backbone derived from the spiro-center or Tröger's base [164]. Li et al. reported a series of spiro-TR-PBOs that contained a spiro-center in the TR-β backbones [175]. The TR process increased the CO_2 permeability by six folds compared to that of the precursor. Hu et al. copolymerized a TR-able poly(hydroxyimide) and a non-TR-able polyimide containing the highly rigid Tröger's base unit as shown in Figure 12 [176]. The synergistic effect between the TR and Tröger's base units resulted in an improved CO_2 permeability of 541 Barrer and a CO_2/CH_4 selectivity of 32, which was significantly higher than the neat TR and PIM counterparts. The mechanical properties of the copolymer were also significantly improved.

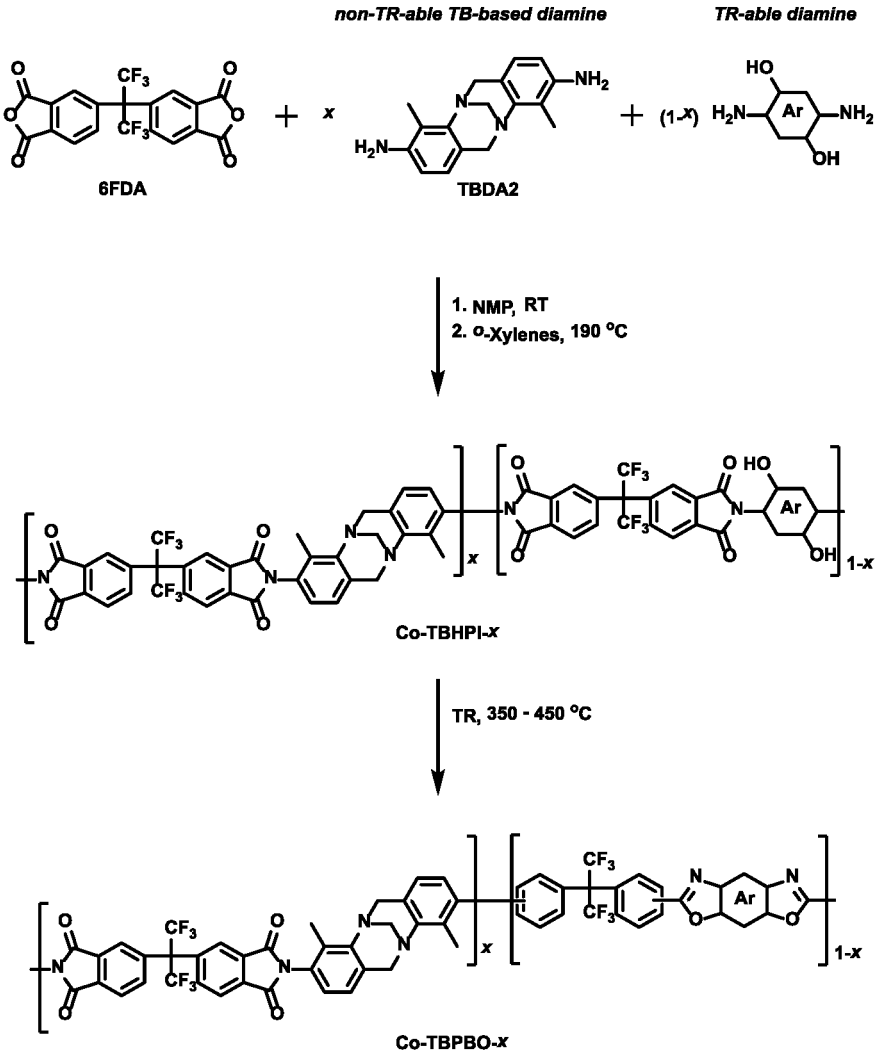

Figure 12. Synthesis of a TR-PBO copolymer containing Tröger's base units. Adapted from Ref. [176]; copyright Elsevier.

Overall, as the state-of-the-art glassy polymers with the highest chain rigidity and cavity uniformity, TR polymers have great potentials in CO_2/CH_4 separation as well as applications in certain CO_2/N_2 separation scenario. Progress has also been witnessed in recent years for the HF membrane synthesis of TR polymers [177-179], which is a key step for increasing the membrane packing density.

3.5. Iptycene-containing polymers

An emerging building block for the synthesis of shape-persisting, rigid polymers is iptycene, which is a class of 3-D molecules with arene rings fused to a [2,2,2]bicyclooctatriene bridgehead [180]. The most commonly utilized iptycenes in gas separation membranes are (1) triptycene (Trip), (2) extended triptycene (exTrip), and (3) pentiptycene (Pent) [181]. As shown in Figure 13, the clefts of the arene "blades" form an internal free volume (IFV, 31 $Å^3$ and 133$Å^3$ for Trip and Pent, respectively) within the iptycene units, which is preserved when built into the polymer backbone and can provide certain size-sieving ability for light gas separation [182,183]. Because of the rigid and shape-persisting nature of the iptycenes, the IFV does not collapse as opposed to other high-free-volume polymers, thus less tendency to physical aging [184].

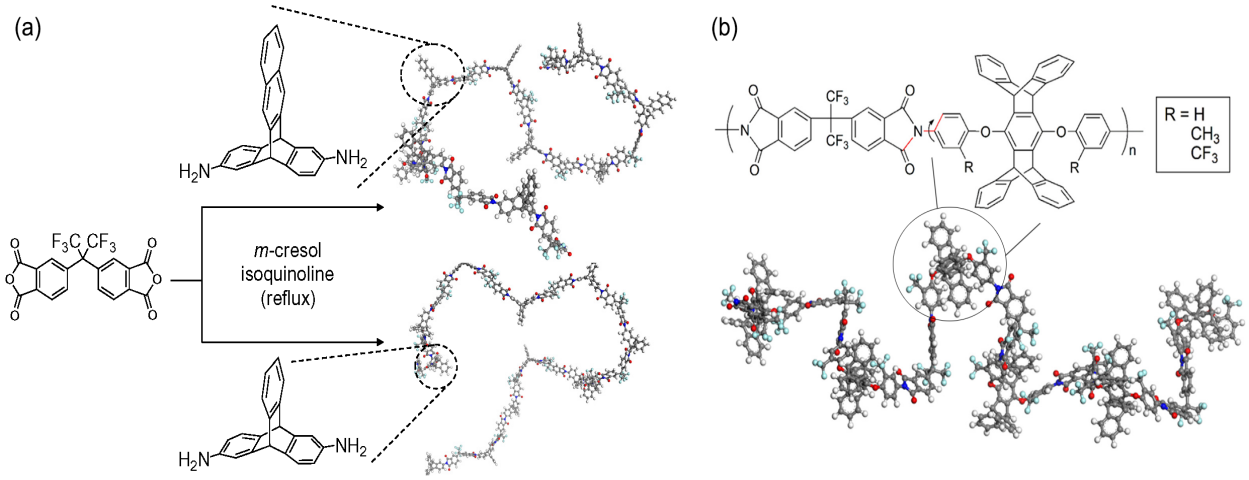

Figure 13. Synthesis of 6FDA-iptycene polyimides by using (a) triptycene and extended triptycene and (b) pentiptycene. Adapted from Refs. [182,183]; copyright Elsevier.

In addition, diverse chemistry is available to change the substituent groups on the iptycenes, and these functional groups can be used in numerous polycondensation reactions to incorporate

the iptycene units in a variety of glassy polymers [185]. Based on the backbone architecture, these iptycene-containing polymers fall into three structures: non-ladder, semi-ladder, and ladder polymers. Table S5 in the SI summarizes the transport properties of representative examples.

The iptycene-containing non-ladder polymers are typically a family of polyimides with the iptycene units introduced by the dianhydride or diamine (see Figure 13). 6FDA has been widely used as the dianhydride to polymerize with 2,6-diaminotriptycene (DAT1) [186], its extended triptycene diamine derivative (DAT2) [182], and pentiptycene diamine (PPDA) [183,187]. Compared to their neat polyimide counterparts, the free volume of these iptycene-polyimides could be increased by ca. 40%, which was beneficial for the gas diffusivity and permeance [182]. Wide-angle X-ray diffraction (WAXD) studies showed that the average interchain spacing of these iptycene-polyimides was in the range of 5–6 Å, which was partially attributed to the IFV of the iptycene units [186]. The CO_2/gas selectivities, however, were not much different compared to the neat polyimides because the retainment of the large cavities caused by the inefficient chain packing.

In order to further refine the cavity size distribution, the triptycene unit was introduced in TR polymers, and the gas separation performances of the derived TR-PBO membranes have been widely studied [188,189]. The triptycene unit was retained during the TR process and improved the size-sieving ability of the TR polymers. A CO_2 permeability of 270 Barrer and an exceptional CO_2/CH_4 selectivity of 67 were registered by an triptycene-containing TR-α polymer [189]. A series of TR-polyimide copolymers containing the triptycene units were also synthesized with the purpose to combine the size-sieving ability of iptycene and the good processibility of TR copolymers [190,191]. In particular, a TR-α-PBO-polyimide copolymer with triptycene units in the TR segments exhibited a high CO_2 permeability of 519 Barrer and a CO_2/CH_4 selectivity of 58

[191]. Because of its potential for the use in natural gas sweetening, the TR conditions, mixed gas sorption, and aging properties of this polymer were extensively studied [192,193].

In order to further increase the interchain spacing and overcome the upper bound trade-off, the imide linkage can be replaced by a more rigid semi-ladder or ladder backbone. In this case, the single-bond connections are partially or completely replaced by two-bond connections with restricted rotation freedom. The archetype for the semi-ladder, iptycene-containing polymers is a series of PIM-polyimide (PIM-PI) copolymers, such as KAUST-PIs [194,195]. As illustrated in Figure 14, these PIM-PIs fused the triptycene unit into the backbone for the restriction of chain rotation. The bridgehead substituent groups on the triptycene unit and the *ortho*-functional group on 6FDA were varied to further tune the free volume and chain packing properties.

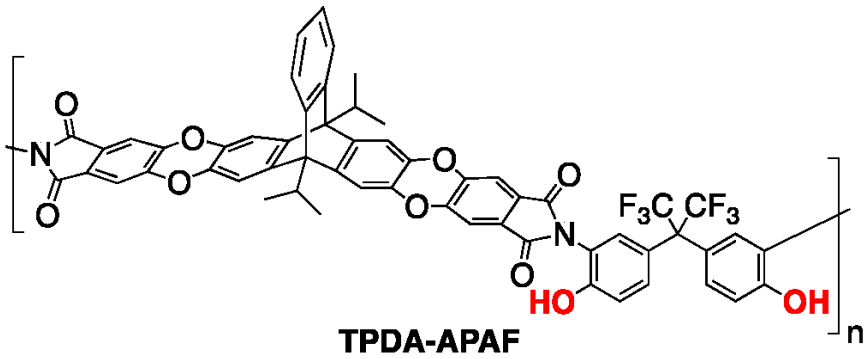

TPDA-APAF

Figure 14. Hydroxyl-functionalized polyimides, derived from 2,2-bis(3-amino-4-hydroxyphenyl)-hexafluoropropane (APAF), containing conventional 6FDA and PIM-type 9,10-diisopropyl-triptycene dianhydrides (TPDA). Adapted from Ref. [196]; copyright Elsevier.

For the polyimides illustrated in Figure 14, Swaidan et al. showed that a diisopropyl-substituted triptycene could significantly stiffen the chain, while the introduction of hydroxyl groups on the 6FDA unit could promote the chain-to-chain interaction via hydrogen bonding [196]. As listed in

Table S5 in the SI, these semi-ladder, triptycene-based PIM-PIs generally exhibited a higher CO_2 permeability but lower CO_2/CH_4 and CO_2/N_2 selectivities compared with the iptycene-based non-ladder polyimides. In addition, a semi-ladder polyimide that did not contain a PIM segment was reported by Mao et al., in which the triptycene unit was introduced by the diamine monomer [197].

The PIM-based semi-ladder polymers discussed above all feature certain contortion in the backbones. In full ladder polymers, however, the backbones are super-rigid and ribbon-like with no contortion. The first few iptycene-containing ladder polymers were synthesized by the homopolymerization of a triptycene-containing monomer that has dihydroxy groups on one end of the monomer and difluoro-functional groups on the other end. These ladder polymers, namely TPIM-1 and TPIM-2, possessed narrow ultra-micropores and a large amount of micropores >10 Å [198].

Other variations containing Tröger's base in the backbones were also reported [199]. Although these ladder polymers were not as permeable as their PIM counterparts, they exhibited a significantly improved CO_2/gas selectivity, likely because of the reduced free volume caused by the π-π interaction between the iptycene units. A recent breakthrough was made by McKeown and coworkers for the synthesis of a series of 2D ladder polymers fused with extended triptycene and its derivatives [52]. Specifically, PIM-BTrip with no substitution on the extended triptycene showed high CO_2/CH_4 and CO_2/N_2 selectivities. In combination with the high CO_2 permeability, the performance of this ladder polymer surpassed both the 2008 Robeson upper bounds for CO_2/CH_4 and CO_2/N_2 separations. Updated upper bounds were proposed based on this series of polymers, which have been referred as the "2019 upper bounds" in the literature.

3.6. Other non-reactive polymers

The compilation of data in Tables S1–S5 in the SI indicates that these non-reactive polymers do not possess sufficient H_2/CO_2 selectivity for applications such as syngas purification. Rubbery membranes such as polyethers and poly(TRIL)s do not exhibit a good H_2/CO_2 selectivity due to the higher CO_2 condensability. The cavity size in the glassy polymers is too large for the size sieving of H_2 against CO_2. Therefore, a H_2/CO_2 selectivity less than 10 is typically observed. However, PBIs are regarded as promising materials for H_2/CO_2 separation due to the inherent strong π-π stacking and hydrogen bonding. PBIs generally have a low FFV in the range of 0.09–0.17 but a decent interchain spacing ca. 4 Å [30]. Hence, a decent H_2/CO_2 selectivity of 10–20 can be achieved at 35°C but the H_2 permeability is only 2–3 Barrer [200-202].

As discussed in Figure 2 (c), the H_2 permeability and H_2/CO_2 selectivity are expected to increase simultaneously with increasing temperature. Such a beneficial effect of operating the PBI membranes at a higher temperature was reported by Li et al. for four commercial PBIs [28] and by Stevens et al. for a tetraaminodiphenylsulfone-based PBI at 250°C [203]. The H_2 permeability could increase to as high as 997 Barrer due to the increased H_2 diffusivity; however, the H_2/CO_2 selectivity was still in the range of 20–30 [28]. In order to further tighten the nanostructure of PBI, Zhu et al. used terephthaloyl chloride (TCL), H_2SO_4, and H_3PO_4 to crosslink a commercial PBI, Celazole® S10 [44,204]. The PBI doped with H_3PO_4 exhibited a narrower interchain spacing of 3.6 Å and demonstrated an unprecedented H_2/CO_2 selectivity of 140 at 150°C.

Another study to increase the chain rigidity and size-sieving ability was reported by Ali et al. via the interfacial polymerization of *m*-phenylenediamine (MPD) and TMC [205]. Compared with conventional reverse osmosis membranes, this crosslinked polyamide was synthesized with a higher diamine-to-acyl chloride ratio, which restricted the interchain spacing to ca. 3.5 Å. In

addition, TFC membrane with a selective layer thickness of 100 nm was prepared. The tight polymer nanostructure and the thinness of the membrane resulted in a H_2 permeance of 350 GPU and a H_2/CO_2 selectivity of ca. 50 at 140°C.

For CO_2/N_2 separation, a new crosslinked polyphosphazene (PPZ) was synthesized by the photopolymerization of a PPZ containing 2-allylphenoxy side groups [206]. Specially, the crosslinked PPZ was judiciously blended with poly[bis(methoxyethoxyethoxy)phosphazene] (MEEP), a low MW PPZ containing a high-content of ether oxygen. This rubbery polymer blend exhibited a high CO_2 permeability of 610 Barrer with a good CO_2/N_2 selectivity of 35 at 40°C. The corresponding TFC membrane demonstrated a CO_2 permeance of 1200 GPU with a CO_2/N_2 selectivity of 31 and did not show any decline in the performance over 2000 h with actual flue gas.

Maroon et al. reported on a similar ether oxygen strategy, in which 2-methoxyethoxy (–OEtOMe) groups were grafted on the ε position of the norbornene rings in a poly(norbornene) (PNB) [207]. The incorporation of ether groups softened the rigid, bicyclic backbone and hence provided certain CO_2/N_2 solubility selectivity. Therefore, a CO_2 permeability of 733 Barrer and a CO_2/N_2 selectivity of 28 was demonstrated, which were more attractive for post-combustion carbon capture than the pristine PNB (a CO_2 permeability of 4371 Barrer but with a low CO_2/N_2 selectivity of 13 [207]).

3.7. Amine-containing FTMs

CO_2-selective FTMs differ from the previously discussed non-reactive polymers in that the CO_2/gas separation is achieved by discriminating the reactivity of the gas pair rather than their size or condensability. For this reason, the separation performance of a FTM is not limited by the upper bound behavior as discussed in Section 2.2. Instead, the design principle pivots on two factors:

(1) the kinetic characteristics of the CO_2–carrier reaction and (2) the mobility and confinement of the carrier in the polymeric membrane. The rich chemical and structural varieties of amines make them the ideal carrier for the synthesis of FTMs [208]. Based on how the amine is confined in the FTM, these carriers can be distinguished into two archetypes: fixed-site carrier and mobile carrier. Table S6 in the SI summarizes the transport properties of selected amine-containing FTMs based on the carrier types.

As fixed-site carriers, polyamines with amino groups either in the polymer backbone or as a pendent groups have been reported to possess facilitated transport feature. The commonly utilized polyamines include polyvinylamine (PVAm) [209], poly(ethyleneimine) (PEI) [210], poly(allylamine) (PAA) [72], polyamidoamine (PAMAM) dendrimer [211], and chitosan [212-214] with a reducing density of amino groups at 23.3 = 23.3 > 18.2 > 11.6 > 5.6 mmol/g, respectively. Limited by the low MW or high crystallinity, PEI, PAA, and chitosan are typically blended with poly(vinyl alcohol) (PVA) or crosslinked PVA in order to be fabricated into a thin film or membrane [72,210]. Extensive hydrogen bonds can be formed between the polyamine and PVA, resulting in a fully miscible blends with no phase separation. The polyamine also serves a plasticizer to disrupt the chain packing of PVA.

In the polyamines, i.e., fixed-site carriers, CO_2 molecules hop among the covalently bonded amino groups, which not only provide a reactive diffusion pathway for CO_2 transport, but also increase the overall chemisorption of CO_2 in the membrane. Therefore, exceptional CO_2/N_2, CO_2/H_2, and CO_2/CH_4 selectivities can be achieved even at an elevated temperature [215]. For low MW polyamines, polyethers and their block copolymers were also reported as good hosts for blending [210]. For instance, chitosan was blended with Pebax® MH 1657, a ether-amide block

copolymer and resulted in a CO_2 permeability of 2884 Barrer and a CO_2/N_2 selectivity of 65 at 85°C [212].

Polyamidoamine (PAMAM) dendrimer, on the other hand, can be blended in crosslinked PVA [211] or copolymerized into the hosting polymer [216]. Taniguchi et al. reported a method to extend a zero-generation PAMAM dendrimer by four glycidyl methacrylate moieties, and the acrylate sites were then copolymerized with poly(ethylene glycol) dimethacrylate (PEGDMA) to form a polymer network containing both ether and amino contents [103]. The resultant polymer exhibited a good membrane forming ability, with a CO_2 permeability of 132 Barrer and a CO_2/H_2 selectivity of 50 at 40°C. This resultant reverse-selective membrane demonstrated a much higher CO_2/H_2 selectivity owing to the facilitated transport of CO_2 in comparison with other rubbery polymers listed in Tables S1 and S2 in the SI.

Among the polyamines used for FTM synthesis, PVAm is known for its highest amino group density and excellent processibility. High MW PVAm can be easily obtained via the free-radical polymerization of *N*-vinylforamide; the resultant vinyl polymer can then be hydrolyzed to afford primary amino groups as pendent groups [217,218]. This hydrophilic polymer can be dissolved in water and coated on an ultrafiltration membrane [219]. The resultant TFC membranes demonstrated a CO_2 permeance greater than 200 GPU and a CO_2/N_2 selectivity higher than 500 [220,221].

It should be noted that the coating of PVAm is not straightforward. This hydrophilic polymer has a poor wettability on most ultrafiltration membranes due to their hydrophobicity. Therefore, hydrophilic modification was performed on the substrate prior to the coating [222-224]. Moreover, TFC membranes with a PVAm selective layer as thin as 100 nm on a polydimethylsiloxane (PDMS) gutter layer was reported by Li et al. with a CO_2 permeance of 1887 GPU and a CO_2/N_2 selectivity

of 83 [225]. In order to improve the adhesion of the PVAm layer, the gutter layer was dip-coated with polydopamine (PDA). Other hydrophilic or amphiphilic moieties, such as PVA [226] and polymeric surfactants [227], have also been used as the compatibilizer between the PVAm selective layer and the substrate.

The primary amino groups on PAA and PVAm can also be modified to introduce sterically hindered amines in FTMs. As discussed in Section 2.3, two primary or secondary amino groups react with a CO_2 molecule following the zwitterion mechanism to form a stable carbamate ion. However, if the amino group is sterically hindered, the rotation of the C–N bond in the carbamate product is restricted and hence the carbamate product is destabilized by the surrounding bulky substituents. In the presence of water, the hindered carbamate can be easily hydrolyzed, resulting in the formation of bicarbonate and the regeneration of a free amino group [228,229]:

$$CO_2 + R_1\text{–}NH\text{–}R_2 \rightleftharpoons R_1R_2\text{–}NH^+\text{–}COO^- \rightleftharpoons R_1R_2\text{–}N\text{–}COOH$$

$$R_1R_2\text{–}N\text{–}COOH + R_1\text{–}NH\text{–}R_2 \rightleftharpoons R_1R_2\text{–}N\text{–}COO^- + R_1R_2\text{–}NH_2^+$$

$$R_1R_2\text{–}N\text{–}COO^- + H_2O \rightleftharpoons R_1\text{–}NH\text{–}R_2 + HCO_3^-$$

Therefore, an equimolar stoichiometry between CO_2 and the amino group can be achieved, thereby doubling the CO_2 loading capacity [72,230].

Zhao and Ho grafted *sec*-butyl, isopropyl, and *tert*-butyl groups on the primary amino sites in PAA [72]. As shown in Figure 15, a moderately hindered PAA, poly(*N*-isopropylallylamine) (PAA-C_3H_7), exhibited a high CO_2 permeability of 297 Barrer, which was nearly 5.5 times more permeable than the unhindered PAA. The improved CO_2 permeability was not attributed to a change in free volume since the CO_2/H_2 selectivity was also increased from 16 to 40 after the hindrance modification. A severely hindered PAA, poly(*N*-*tert*-butylallylamine) (PAA-$C(CH_3)_3$), however, showed a lower CO_2 permeability and selectivity. In this case, the severe steric hindrance

restricted the collision orientation between the amino group and CO_2 due to the bulky substituents surrounding the amino site. Therefore, the reaction kinetics was slower than the less hindered counterparts [72].

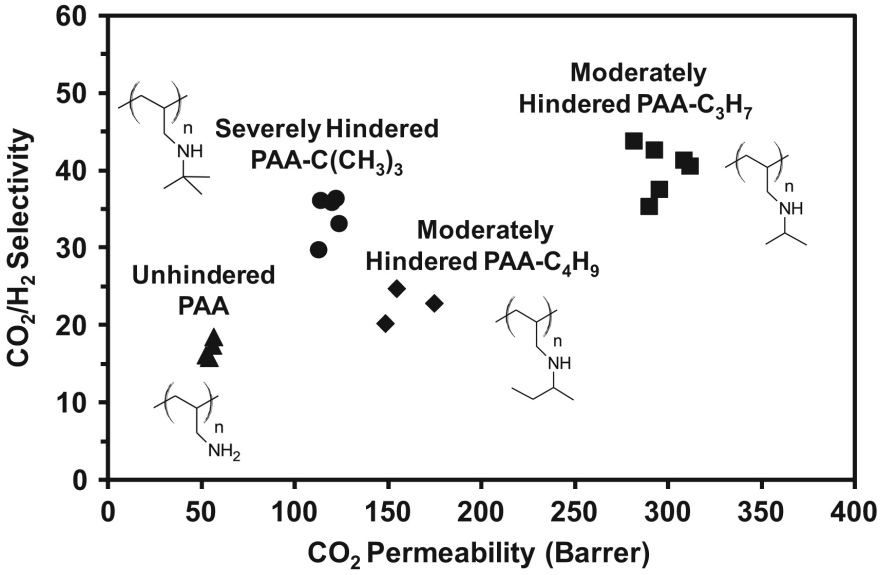

Figure 15. CO_2/H_2 selectivities and CO_2 permeabilities of FTMs containing 70 wt.% sterically hindered PAA and 30 wt.% crosslinked PVA at 110°C. Adapted from Ref. [72]; copyright Elsevier.

A similar strategy was also adopted by Tong and Ho to synthesize *N*-substituted PVAm with methyl, isopropyl, and *tert*-butyl groups [230]. Because of the inherent hindrance from the vinyl backbone on the amino groups, an *N*-methyl substitution yielded sufficient steric hindrance and resulted in the highest CO_2 permeability of 264 Barrer at 57°C. When the temperature was increased to 102°C, the hindered PVAm exhibited an enhanced CO_2 permeability of 6804 Barrer with an exceptional CO_2/H_2 selectivity of 162.

Tertiary amines were also utilized as fixed-site carriers in FTMs synthesis. An innovative approach was proposed by Li et al., where interfacial polymerization was conducted for TMC and 3,3′-diamino-*N*-methyldipropylamine (DNMDAm), a multi-amine with two terminal primary amino groups and a tertiary amino group [231]. As shown in Figure 16, TMC exhaustively reacted with the terminal amino groups on DNMDAm but was nonreactive to the tertiary amino group. Therefore, a crosslinked polymer with tertiary amino groups were formed. The TFC membrane showed a high CO_2 permeance of 1613 GPU with a CO_2/N_2 selectivity of 138 at 30°C. This facile membrane formation method was also used to synthesize fixed-site carrier membranes with other multi-amine monomers [232,233].

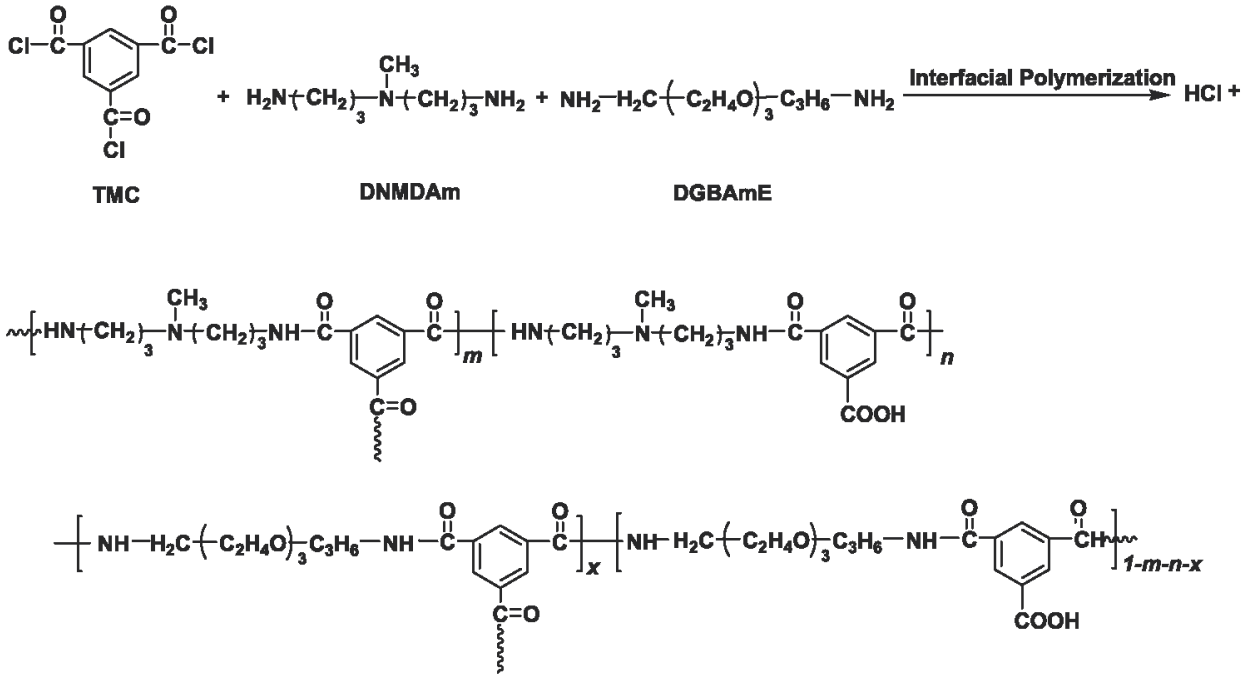

Figure 16. Interfacial polymerization of TMC and DNMDAm for the synthesis of TFC membrane containing tertiary amino groups. Adapted from Ref. [231]; copyright Wiley.

The addition of small molecular amine in a compatible polymer was proposed and demonstrated for CO_2 separation in polymeric membranes by Ho [234,235] and subsequently studied extensively by his coworkers and him [6,18,72,77,218,236-247]. Compared with the fixed-site carrier membranes, the incorporation of mobile carrier adds another flexibility to introduce high-content, sophisticated amine structures in the membrane. In addition to their high diffusivities, these small molecules can also plasticize the hosting polymer, resulting in a higher gas diffusivity in the membrane. For instance, ethylenediamine (EDA) [248] and monoethanolamine (MEA) [249] were blended in PVAm and coated on porous substrate to form TFC membranes. These membranes demonstrated a CO_2 permeance >600 GPU with a CO_2/N_2 selectivity >100 and a CO_2/H_2 selectivity >60. However, although these multi-amines can form hydrogen bonds with PVAm, they can leave the membrane due to their high volatility and thus cause membrane instability.

An alternative type of mobile carrier was first proposed by Ho [234,235] using nonvolatile aminoacid salts; for example, his group deprotonated 2-aminoisobutyric acid (AIBA) with KOH [18,77,236]. The resultant aminoacid salt AIBA-K contained a sterically hindered primary amino group as well as an ionic pair between the carboxylic group and the potassium ion. This mobile carrier has been blended with sulfonated polybenzimidazole (SPBI) [236], PAA-C_3H_7 [77], and PVAm [18], rendering a CO_2 permeability greater than 1000 Barrer and a high CO_2/H_2 selectivity as high as 300 at 100–110°C. Owing to the high ionic strength, the AIBA-K aminoacid salt was nonvolatile at the operating temperature, and a good membrane stability was demonstrated by these FTMs.

Inspired by this work, a number of aminoacid salts have been designed and utilized for FTM synthesis. Specially, less sterically hindered aminoacids have also been used in the carrier

synthesis for CO_2/N_2 separation, including the glycine (Gly), proline (Pro), and cysteine (Cys) [218,237,250]. After the deprotonation by a strong base (e.g., KOH), these mobile carriers were incorporated in PVAm and PVA with a content as high as 65 wt.%. The resultant TFC membranes demonstrated a CO_2 permeance ca. 1100 GPU and a CO_2/N_2 selectivity greater than 170.

The aminoacid salt can also be synthesized by using a multi-amine, rather than an inorganic base, to deprotonate the aminoacid. Han and coworkers proposed the deprotonation of an α-aminoacid, such as Gly and sarcosine (Sar), with a cyclic multi-amine, such as piperazine (PZ) and 2-(1-piperazinyl)ethylamine (PZEA), to form an aminoacid salt (e.g., PZ-Gly and PZEA-Sar) with multiple free amino groups [238].

As shown in Figure 17 (a)–(d), DFT calculations suggested that for PZ-Gly, the primary amino group on Gly is responsible for the reaction of PZ-Gly with CO_2; on the other hand, for PZEA-Sar, the primary amino group on PZEA and the secondary amino group on Sar partake in the reaction with CO_2 following the carbamate and bicarbonate pathways, respectively [241]. Further reaction coordinates analysis shows that PZ-Gly and PZEA-Sar have a higher reactivity towards CO_2 than PVAm (see Figure 17 (e) and (f)). In addition, PZEA-Sar exhibits a faster reaction kinetics than PZ-Gly following the carbamate pathway, and it also has a higher tendency to induce the bicarbonate formation. Therefore, a higher CO_2 loading capacity can be expected for PZEA-Sar [241].

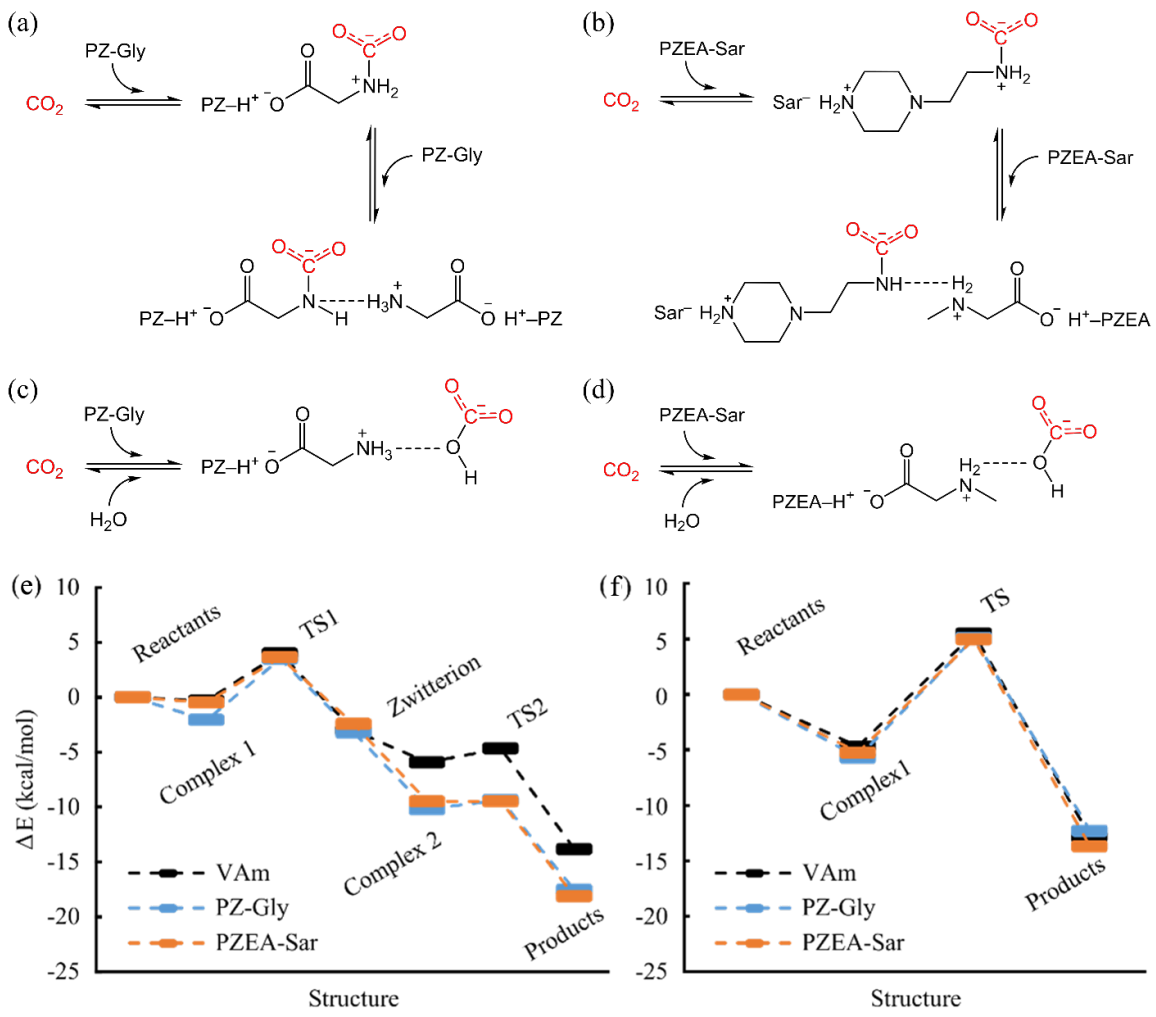

Figure 17. The carbamate pathways of (a) PZ-Gly and (b) PZEA-Sar and the bicarbonate pathways of (c) PZ-Gly and (d) PZEA-Sar for leading to their preferred products. Relative energies (ΔE, with respect to reactants) of structures in the amine–CO_2 reactions of carriers following the (e) carbamate and (f) bicarbonate pathways. Adapted from Ref. [241]; copyright ACS.

Membrane formation studies indicated that PVAm was miscible with up to at least 85 wt.% PZEA-Sar, likely owing to the bulky $PZEA^+$ cation and the resultant low tendency for crystallization and salting-out issues [239]. The corresponding TFC membrane exhibited a CO_2 permeance of 1450 GPU and a CO_2/N_2 selectivity >160 at 67°C. The facile fabrication of this

FTM containing PZEA-Sar was also demonstrated by a roll-to-roll continuous process [242-244], and the membrane was rolled into prototype spiral-wound (SW) membrane modules with a high packing density [245,246]. The module was tested with actual flue gas at the National Carbon Capture Center (NCCC), Wilsonville, AL, USA, and demonstrated a 500-h stability in the presence of 2 ppm SO_2, 1.5–4 ppm NO_2, and 7.6% O_2 [247]. PZEA-Sar was also incorporated in a polymer blend containing PVA, PAA-C_3H_7, and a surface-modified nanocellulose by Janakiram et al. [251]. The TFC membrane showed a CO_2 permeance of 652 GPU with a CO_2/N_2 selectivity of 41 at 35°C.

A special note is needed for the reporting and comparison of the transport results of FTMs. It is known that the CO_2 permeance (or permeability) of a FTM is dependent on the CO_2 partial pressure due to the carrier saturation phenomenon [67,252]. One example is shown in Figure 18 (a), where the CO_2 permeance of a FTM containing PZEA-Sar reduced significantly with increasing CO_2 partial pressure [253]. The initial non-linear decrease of CO_2 permeance was caused by the consumption of free amine carriers by the CO_2-amine reaction in the membrane, followed by a plateau when all the carriers were reacted. The strong concentration dependance suggests that membrane performance measured for low-pressure applications (e.g., carbon capture from flue gas) cannot be projected for high-pressure applications (e.g., syngas purification and natural gas sweetening). For this reason, the synthesis of FTM is task-specific, and the range of CO_2 partial pressure affects the choice of amine carrier.

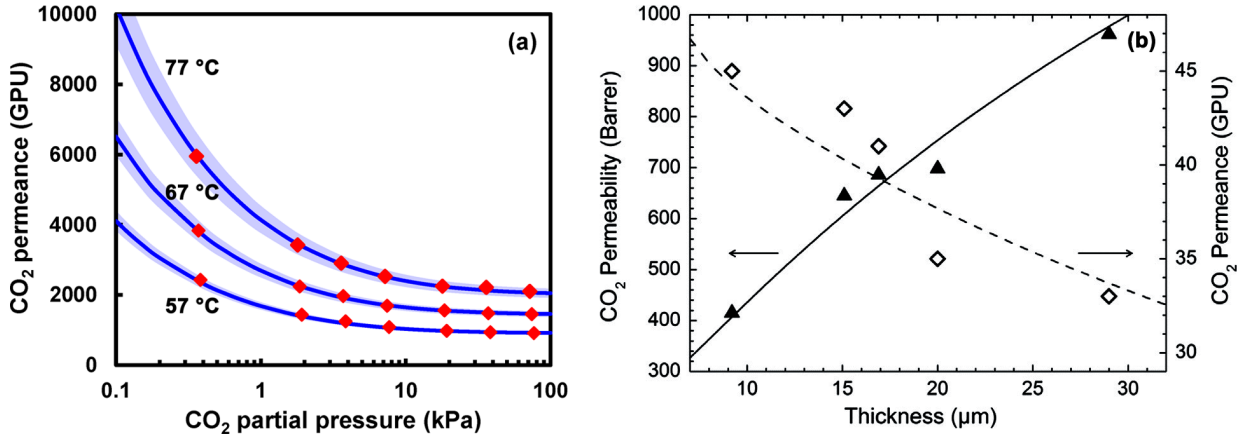

Figure 18. (a) Effect of CO_2 partial pressure on the CO_2 permeance of a FTM containing PZEA-Sar; adapted from Ref. [253]; copyright ACS. (b) Effects of membrane thickness on the CO_2 permeability and permeance of a FTM containing AIBA-K. Adapted from Ref. [254]; copyright Elsevier.

The CO_2 permeability of a FTM also depends on the membrane thickness. CO_2 molecules react with the amine carriers at the feed/membrane interface and are released at the membrane/permeate interface by the reverse reaction. The forward and reverse reaction kinetics can impose certain mass transfer resistances at the two interfaces, which are independent of the membrane thickness [239,255-257]. As shown in Figure 18 (b), the CO_2 permeability reduced with reducing membrane thickness due to the persistent interfacial resistances [254]. As a consequence, the CO_2 permeance increased non-linearly with decreasing membrane thickness. In general, the CO_2 permeability measured by a thick film cannot be extrapolated to estimate the CO_2 permeance of the corresponding facilitated-transport TFC membrane. In this sense, CO_2 permeance is a more meaningful measure of the FTM performance. Thus, we recommend that both the CO_2 permeance and CO_2 permeability should be reported for new FTM materials and that the results should be accompanied by the membrane architecture and testing conditions.

3.8. FTMs with other carriers

Carriers other than amine have also been used for the synthesis of FTMs, and they include other organic bases (e.g., quaternary ammonium hydroxide and carbonate, amidine, carboxylate), CO_2 hydration catalyst, and mimic enzymes (e.g., Zn-cyclen and vinylimidazole-zinc complex). The CO_2/gas transport performances of relevant examples are listed in Table S7 in the SI.

Similar to the reaction with a tertiary amine (see Section 2.3), CO_2 can react with other Brønsted bases or catalyzed water to form bicarbonate or carbonate as the product. These reactions tend to be slower than the amine–CO_2 reaction but can be utilized to facilitate the CO_2 transport in situations where the oxidative stability of amine is of concern. A niche application of FTMs is to selectively remove CO_2 and recover H_2 from the anode exhaust of a syngas-air solid oxide fuel cell (SOFC). Because the anode exhaust is at a temperature around 120°C but not at pressure, a sweep air is an economic choice to provide the transmembrane driving force [258]. However, amine-containing FTMs are unstable in this condition due to the oxidation of amine at such a high temperature [259-261]. In order to address this issue, a series of FTMs based on poly(diallyldimethylammonium hydroxide) (PDADMQ-OH) and poly(diallyldimethylammonium fluoride) (PDADMQ-F) were developed by Vakharia et al., in which tetramethylammonium hydroxide (TMAOH) was added as the mobile carrier [262]. The quaternary ammonium hydroxide groups reacted with CO_2 to form bicarbonate, and the fluoride ion catalyzed the water–CO_2 reaction. These FTMs were quite stable under air sweep and demonstrated a CO_2/H_2 selectivity ca. 100 at 120°C.

In order to further increase the membrane selectivity, tetrafluoroboric acid (TBFA) was incorporated in the FTM to further catalyze the water–CO_2 reaction [263]. This improved FTM exhibited a better CO_2/H_2 selectivity of 115, but a thermal degradation was observed when this

membrane was subject to a temperature fluctuation between 120 and 130°C. Kai et al. later demonstrated that the thermal instability stemmed from the Hofmann rearrangement of the tetramethylammonium ion in the presence of hydroxide [264,265], and proposed to use tetramethylammonium fluoride (TMAF) as a mobile catalyst to replace the TMAOH [266]. As shown in Figure 19 (a), TMAF exhibited a desirable thermal stability at 130°C, and it could induce a considerable deshielding of the hydrogen atoms of water as compared to other inorganic fluoride salts (Figure 19 (b)). The nearly "naked" proton in the water molecule enhanced the kinetics of the water–CO_2 reaction, and eventually resulted in a reasonably stable CO_2 permeance of 108 GPU and a CO_2/H_2 selectivity of 106.

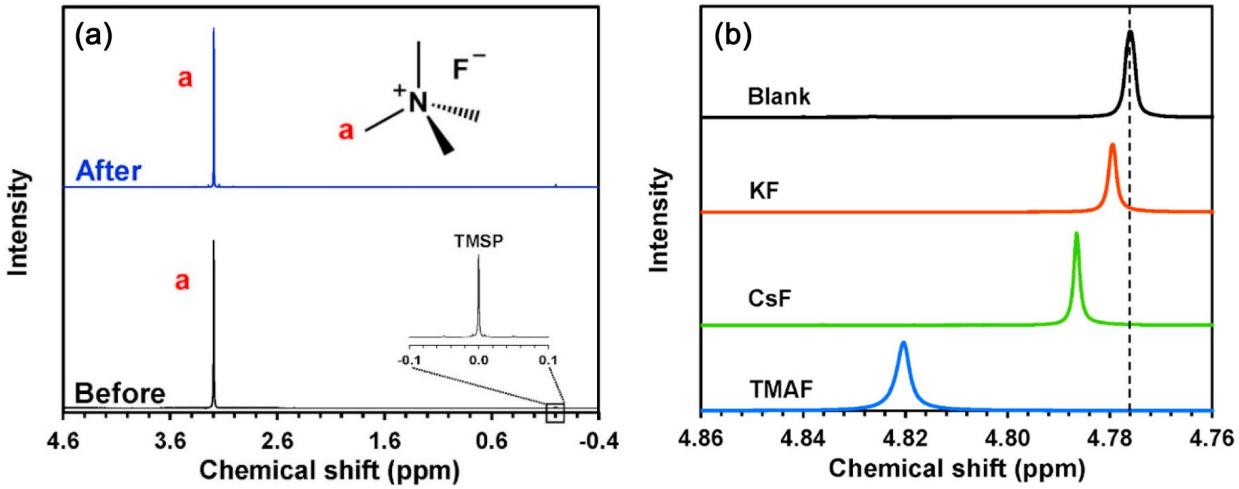

Figure 19. (a) ^{1}H NMR spectra of 0.5 M tetramethylammonium fluoride (TMAF) before and after heating at 130°C; (b) chemical shifts of water in the presence of 0.5 M of KF, CsF, and TMAF. Adapted from Ref. [266]; copyright Elsevier.

Another approach to utilize hydroxide ion as the mobile carrier was reported by Xiong et al. for a hydroxide-exchange membrane with a polysulfone-methylene quaternary phosphonium

backbone [267]. The membrane showed a high CO_2 permeability of 1090 Barrer and a CO_2/N_2 selectivity of 275 when it was fully hydrated. Other organic strong bases, such as amidine [268] and guanidine [269] were also shown to facilitate the CO_2 transport. Blinova and Svec modified a polyaniline (PANI) membrane by the grafting of guanidine groups, which improved the CO_2 permeability to 2460 Barrer with a CO_2/CH_4 selectivity of 540 at 1 atm and 25°C [269]. The membrane performance could be interesting for the methane recovery from biogas. Weak Brønsted bases, such as carbonate [270] and carboxylate ions [271,272] were also incorporated in FTMs in the forms of mobile and fixed-site carriers. Although less reactive than amines, these carriers are advantageous in their better oxidative and chemical stability.

Lastly, bio-inspired FTMs were constructed based on carbonic anhydrase (CA), a metalloenzyme that catalyzes the interconversion between carbon dioxide and water and the dissociated ions of carbonic acid in biological processes. The active size of most CAs is a Zn^{2+} ion coordinates to three histidine groups [273]. Mimic enzymes were constructed by impregnating Zn^{2+} into cyclen, an aza-crown ether. These mimic enzymes were incorporated in PVA, and the resultant FTMs showed a CO_2 permeance of 200–400 GPU with a CO_2/N_2 selectivity ca. 100 [274,275]. Alternatively, poly(*N*-vinyl imidazole) (PVIm) was shown to form a $[(H_2O)Zn(imidazole)_n]^{2+}$ complex and promote the hydration of CO_2 [276]. This feature bestowed the FTM a high CO_2 permeance of 1122 GPU and a CO_2/N_2 selectivity of 83 at 25°C.

4. Concluding Remarks

Since the first commercial membrane gas separation unit was built by Monsanto in 1979, material and membrane research has led to the fast expansion of polymeric membranes into the existing and emerging markets of several key energy-intensive separations, such as post-

combustion carbon capture (CO_2/N_2), syngas purification (CO_2/H_2), and natural gas and biogas sweetening (CO_2/CH_4). In order to compare the many families of polymers reviewed in this paper, the permeability-selectivity data in Tables S1–S7 in the SI are plotted in Figure 20 (a)–(d) against their respective upper bounds.

For CO_2/N_2 separation (Figure 20 (a)), rubbery polymers featuring a high CO_2/N_2 solubility selectivity are advantageous compared with the size-sieving glassy polymers. Polyethers and poly(RTIL)s are promising materials for the decarbonization of flue gas due to a combination of high CO_2 permeability and decent CO_2/N_2 selectivity. FTMs are of particular interest for this application because they generally exhibit a CO_2/N_2 selectivity above the 2008 and 2019 upper bounds. In addition, FTMs are less prone to suffer from carrier saturation in flue gas conditions due to the low CO_2 concentration.

For CO_2/H_2 separation, reverse-selective membranes such as polyethers can offer a CO_2/H_2 selectivity of 10–20 based on the solubility selectivity. A better CO_2/H_2 selectivity of 100–200 can be realized by using FTMs. An advantage of FTMs over polyethers is that they can be operated at an elevated temperature, which is typical for syngas purification and fuel cell applications. In comparison, the CO_2/H_2 selectivity of polyethers is predicted to reduce as shown in Figure 20 (b) due to the reduced solubility selectivity with increasing temperature.

Glassy polymers with size-sieving ability generally exhibit a H_2 selectivity over CO_2. The high-free-volume, shape-persisting polymers possess a high H_2 permeability but a low H_2/CO_2 selectivity because of their large cavity size. Crosslinked PBIs, on the other hand, show a better H_2/CO_2 selectivity but a lower H_2 permeability. As shown in Figure 20 (c), the H_2 selectivity of PBIs can be further improved at a higher temperature. Therefore, PBIs can potentially be used in high-temperature syngas purification where the transmembrane driving force is abundant.

For CO_2/CH_4 separation, conventional and iptycene-containing TR polymers are currently the membrane-to-beat owing to their high CO_2/CH_4 selectivity and relatively slower physical aging. The state-of-the-art TR polymers actually exhibit CO_2/CH_4 separation performance above the 2008 upper bound as shown in Figure 20 (d). Certain perfluorodioxolanes also possess a CO_2/CH_4 selectivity of interest. More importantly, their chemical and plasticization resistances are well suited for natural gas sweetening. FTMs can also exhibit a decent CO_2/CH_4 selectivity, but the risk of carrier saturation makes the current FTMs be more feasible for low-pressure applications such as biogas sweetening.

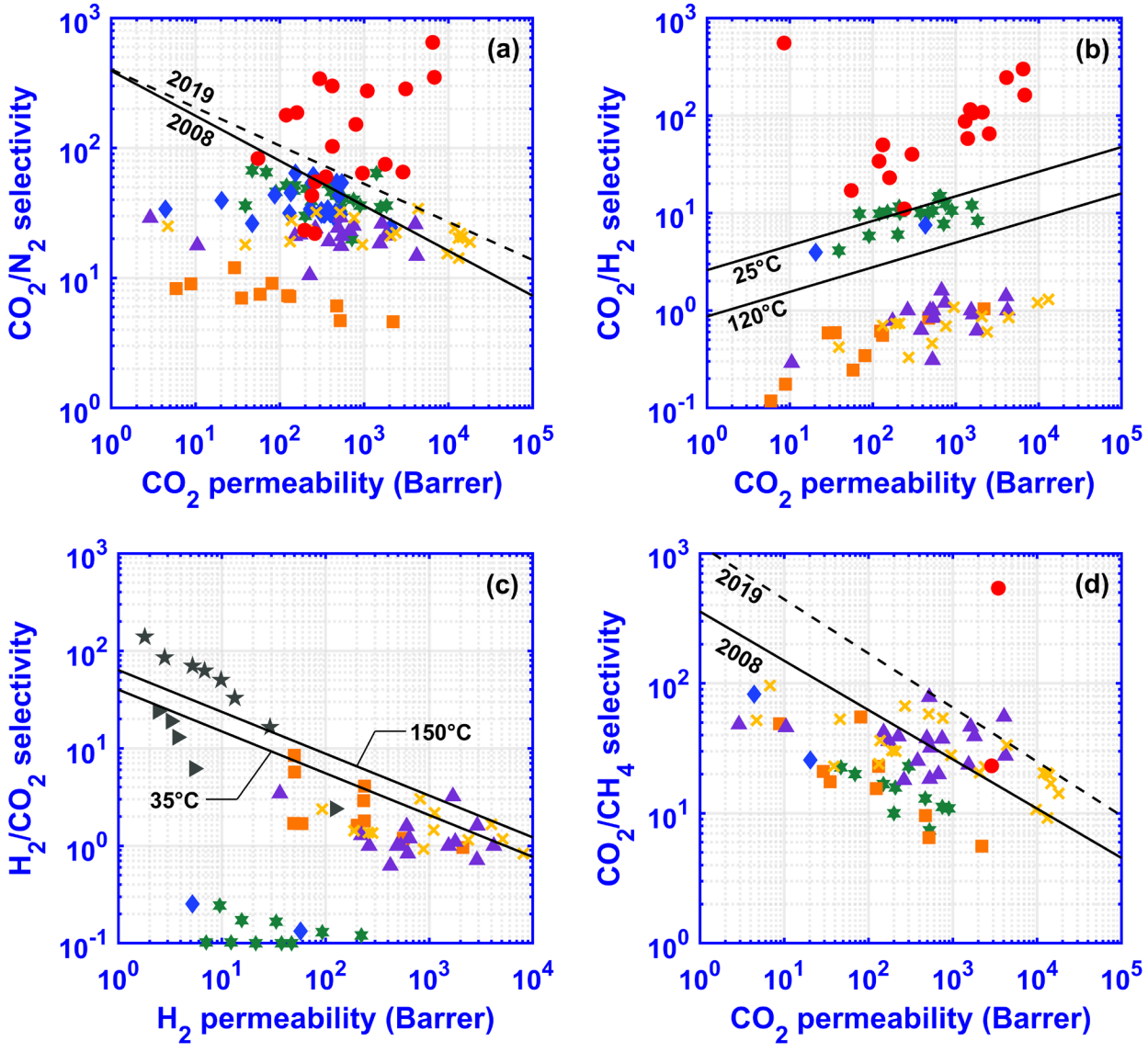

Figure 20. Transport properties of selected polymers against the (a) 2008 [51] and 2019 [52] CO_2/N_2 upper bounds, (b) theoretical CO_2/H_2 upper bounds at 25 and 120°C [53,81], (c) 2008 H_2/CO_2 upper bound [51] and its theoretical projection at 150°C [204], and (d) 2008 [51] and 2019 [52] CO_2/CH_4 upper bounds. Symbols: polyethers (★); poly(RTIL)s (♦); perfluoropolymers (■); TR polymers (▲); iptycene-containing polymers (×); FTMs (●); PBIs at 35°C (►); PBIs at 150°C (★).

As for the future research directions for CO_2 separation and capture, CO_2/N_2 separation from dilute flue gases remains as the most challenging application. New membranes with a CO_2 permeance greater than 3000 GPU are desired to make them more competitive with other carbon capture technologies. In order to achieve this goal, novel membrane materials including new CO_2 carriers and CO_2-philic polymers should be developed, and advanced membrane formation methods are required to realize the potential in a TFC configuration. For CO_2/H_2 separation, FTMs have the potential for syngas purification due to their exceptional CO_2/H_2 selectivity at a temperature greater than 100°C. However, new strategies should be devised to mitigate the carrier saturation at a high CO_2 partial pressure. In view of the chemical and plasticization resistances, the molecular design of perfluorodioxolanes should be further explored for CO_2/CH_4 separation. In particular, the role of fluorine content on gas sorption properties should be elucidated. The knowledge gained is also beneficial for the rational design of other fluorine-containing glassy polymers such as fluorinated polyimides, TR, and triptycene-based polymers.

Acknowledgments

We would like to thank Isaac Andy Aurelio, Katharina Daniels, José D. Figueroa, Krista Hill, and David Lang of the U.S. Department of Energy - National Energy Technology Laboratory (DOE-NETL) and Randy Keefer and Matthew Usher of American Electric Power for their invaluable inputs and helpful discussions for this work. We gratefully acknowledge the funding from DOE/NETL (DE-FE0031635 and DE-FE0031731) and the Ohio Development Services Agency (OER-CDO-D-19-12 and OER-CDO-D-19-13). This work was partly supported by the Department of Energy under Award Numbers DE-FE0031635 and DE-FE0031731 with substantial involvement of the National Energy Technology Laboratory, Pittsburgh, PA, USA.

Nomenclature

a	parameter in Eq. (6)
b	parameter in Eq. (6)
c	parameter in Eq. (7)
D	gas diffusivity in polymer
d	kinetic diameter
E_D	activation energy of diffusion
f	parameter in Eq. (7)
J	flux
ℓ	membrane thickness
M	parameter in Eq. (4)
N	parameter in Eq. (4)
P	gas permeability
Δp	transmembrane partial pressure differential
R	ideal gas constant
S	gas solubility in polymer
T	absolute temperature

Greek letters

ε_i/k	Lennard-Jones temperature
α	ideal selectivity
β	parameter in Eq. (9)
λ	parameter in Eq. (9)

Subscripts

i	species i, i = CO_2, H_2, N_2, or CH_4
j	species j, j = CO_2, H_2, N_2, or CH_4

References

[1] W. Bollinger, D. MacLean, R. Narayan, Separation systems for oil refining and production, Chem. Eng. Prog. 78 (1982).

[2] W.S.W. Ho, K.K. Sirkar, Membrane Handbook, reprint ed., Kluwer Academic Publishers, Boston, 2001.

[3] R.W. Baker, K. Lokhandwala, Natural gas processing with membranes: An overview, Ind. Eng. Chem. Res. 47 (2008) 2109–2121.

[4] R.W. Baker, Membrane Technology and Applications, 3rd ed., John Wiley & Sons, 2012.

[5] R.W. Baker, Future directions of membrane gas separation technology, Ind. Eng. Chem. Res. 41 (2002) 1393–1411.

[6] K. Ramasubramanian, Y. Zhao, W.S.W. Ho, CO_2 capture and H_2 purification: Prospects for CO_2-selective membrane processes, AIChE J. 59 (2013) 1033–1045.

[7] B. Metz, O. Davidson, H. De Coninck, M. Loos, L. Meyer, IPCC Special Report on Carbon Dioxide Capture and Storage. Prepared by Working Group III of the Intergovernmental Panel on Climate Change, IPCC, Cambridge University Press: Cambridge, United Kingdom and New York, USA, 2005.

[8] V. Masson-Delmotte, P. Zhai, H.-O. Pörtner, D. Roberts, J. Skea, P.R. Shukla, A. Pirani, W. Moufouma-Okia, C. Péan, R. Pidcock, S. Connors, J.B.R. Matthews, X. Zhou, M.I. Gomis, E. Lonnoy, T. Maycock, M. Tignor, T. Waterfield, Global Warming of 1.5 °C: An IPCC Special Report on the Impacts of Global Warming of 1.5 °C above Pre-industrial Levels and Related Global Greenhouse Gas Emission Pathways, in the Context of Strengthening the Global Response to the Threat of Climate Change, Sustainable Development, and Efforts to Eradicate

Poverty, Report Number: IPCC SR1.5, Intergovernmental Panel on Climate Change, Incheon, Republic of Korea, 2018.

[9] J.D. Figueroa, T. Fout, S. Plasynski, H. McIlvried, R.D. Srivastava, Advances in CO_2 capture technology—the U.S. Department of Energy's carbon sequestration program, Int. J. Greenh. Gas Con. 2 (2008) 9–20.

[10] R.L. Miller, G.A. Schmidt, L.S. Nazarenko, N. Tausnev, S.E. Bauer, A.D. DelGenio, M. Kelley, K.K. Lo, R. Ruedy, D.T. Shindell, CMIP5 historical simulations (1850–2012) with GISS ModelE2, J. Adv. Model. Earth Syst. 6 (2014) 441–477.

[11] M.A. Barteau, J. Dunn, D. Allen, M.D. Burkart, A.M. Gaffney, R. Gupta, N. Hazari, M. Kanan, P. Kenis, H. Klee, Gaseous Carbon Waste Streams Utilization: Status and Research Needs, AGUFM 2018 (2018) GC41A–03.

[12] U.S. Energy Information Administration, Annual Energy Outlook 2020, January 29, 2020. Website: https://www.eia.gov/outlooks/aeo/.

[13] T. Fout, A. Zoelle, D. Keairns, M. Turner, M. Woods, N. Kuehn, V. Shah, V. Chou, L. Pinkerton, Cost and Performance Baseline for Fossil Energy Plants Volume 1a: Bituminous Coal (PC) and Natural Gas to Electricity Revision 3, U.S. Department of Energy, Report Number: DOE/NETL-2015/1723, Washington, DC, USA, 2015.

[14] T.C. Merkel, X. Wei, Z. He, L.S. White, J. Wijmans, R.W. Baker, Selective exhaust gas recycle with membranes for CO_2 capture from natural gas combined cycle power plants, Ind. Eng. Chem. Res. 52 (2012) 1150–1159.

[15] K. Ramasubramanian, H. Verweij, W.S.W. Ho, Membrane processes for carbon capture from coal-fired power plant flue gas: A modeling and cost study, J. Membr. Sci. 421 (2012) 299–310.

[16] T.C. Merkel, H. Lin, X. Wei, R. Baker, Power plant post-combustion carbon dioxide capture: An opportunity for membranes, J. Membr. Sci. 359 (2010) 126–139.

[17] T. Fout, A. Zoelle, D. Keairns, M. Turner, M. Woods, N. Kuehn, V. Shah, V. Chou, L. Pinkerton, J. Black, Cost and Performance Baseline for Fossil Energy Plants Volume 1b: Bituminous Coal (IGCC) to Electricity Revision 2b—Year Dollar Update, U.S. Departmeant of Energy, Report Number: DOE/NETL-2015/1727, Washington, DC, USA, 2015.

[18] V. Vakharia, K. Ramasubramanian, W.S.W. Ho, An experimental and modeling study of CO_2-selective membranes for IGCC syngas purification, J. Membr. Sci. 488 (2015) 56–66.

[19] T.C. Merkel, M. Zhou, R.W. Baker, Carbon dioxide capture with membranes at an IGCC power plant, J. Membr. Sci. 389 (2012) 441–450.

[20] J.D. Wind, D.R. Paul, W.J. Koros, Natural gas permeation in polyimide membranes, J. Membr. Sci. 228 (2004) 227–236.

[21] F. Ahmad, K.K. Lau, A.M. Shariff, Y. Fong Yeong, Temperature and pressure dependence of membrane permeance and its effect on process economics of hollow fiber gas separation system, J. Membr. Sci. 430 (2013) 44–55.

[22] M. Scholz, T. Harlacher, T. Melin, M. Wessling, Modeling gas permeation by linking nonideal effects, Ind. Eng. Chem. Res. 52 (2012) 1079–1088.

[23] S. Basu, A.L. Khan, A. Cano-Odena, C. Liu, I.F. Vankelecom, Membrane-based technologies for biogas separations, Chem. Soc. Rev. 39 (2010) 750–768.

[24] H. Lin, B.D. Freeman, Materials selection guidelines for membranes that remove CO_2 from gas mixtures, J. Mol. Struct. 739 (2005) 57–74.

[25] S. Kilic, S. Michalik, Y. Wang, J. Johnson, R. Enick, E. Beckman, Effect of grafted Lewis base groups on the phase behavior of model poly(dimethyl siloxanes) in CO_2, Ind. Eng. Chem. Res. 42 (2003) 6415–6424.

[26] Z. Tong, W.S.W. Ho, Facilitated transport membranes for CO_2 separation and capture, Sep. Sci. Technol. 52 (2017) 156–167.

[27] M.W. Uddin, M.-B. Hägg, Effect of monoethylene glycol and triethylene glycol contamination on CO_2/CH_4 separation of a facilitated transport membrane for natural gas sweetening, J. Membr. Sci. 423 (2012) 150–158.

[28] X. Li, R.P. Singh, K.W. Dudeck, K.A. Berchtold, B.C. Benicewicz, Influence of polybenzimidazole main chain structure on H_2/CO_2 separation at elevated temperatures, J. Membr. Sci. 461 (2014) 59–68.

[29] K.A. Berchtold, R.P. Singh, J.S. Young, K.W. Dudeck, Polybenzimidazole composite membranes for high temperature synthesis gas separations, J. Membr. Sci. 415–416 (2012) 265–270.

[30] L. Hu, S. Pal, H. Nguyen, V. Bui, H. Lin, Molecularly engineering polymeric membranes for H_2/CO_2 separation at 100–300 °C, J. Polym. Sci. 58 (2020) 2467–2481.

[31] M.S. Suleman, K.K. Lau, Y.F. Yeong, Plasticization and swelling in polymeric membranes in CO_2 removal from natural gas, Chem. Eng. Technol. 39 (2016) 1604–1616.

[32] Y. Han, W.S.W. Ho, Recent developments on polymeric membranes for CO_2 capture from flue gas, J. Polym. Eng. 40 (2020) 529–542.

[33] P. Hao, J. Wijmans, Z. He, L.S. White, Effect of pore location and pore size of the support membrane on the permeance of composite membranes, J. Membr. Sci. (2019) 117465.

[34] L. Zhu, M. Yavari, W. Jia, E.P. Furlani, H. Lin, Geometric restriction of gas permeance in ultrathin film composite membranes evaluated using an integrated experimental and modeling approach, Ind. Eng. Chem. Res. 56 (2016) 351–358.

[35] J. Wijmans, P. Hao, Influence of the porous support on diffusion in composite membranes, J. Membr. Sci. 494 (2015) 78–85.

[36] J. Wijmans, R. Baker, The solution-diffusion model: A review, J. Membr. Sci. 107 (1995) 1–21.

[37] V. Bondar, B. Freeman, I. Pinnau, Gas transport properties of poly (ether-*b*-amide) segmented block copolymers, J. Polym. Sci. Part B: Polym. Phys. 38 (2000) 2051–2062.

[38] L.M. Robeson, Z.P. Smith, B.D. Freeman, D.R. Paul, Contributions of diffusion and solubility selectivity to the upper bound analysis for glassy gas separation membranes, J. Membr. Sci. 453 (2014) 71–83.

[39] D.W. Breck, Zeolite Molecular Sieves: Structure, Chemistry and Use, John Wiley & Sons, New York, NY, 1973.

[40] B.D. Freeman, Basis of permeability/selectivity tradeoff relations in polymeric gas separation membranes, Macromolecules 32 (1999) 375–380.

[41] R. Barrer, Diffusion in elastomers, Kolloid-Zeitschrift 120 (1951) 177–190.

[42] R. Barrer, G. Skirrow, Transport and equilibrium phenomena in gas–elastomer systems. I. Kinetic phenomena, J. Polym. Sci. 3 (1948) 549–563.

[43] R. Barrer, Diffusivities in glassy polymers for the dual mode sorption model, J. Membr. Sci. 18 (1984) 25–35.

[44] L. Zhu, M.T. Swihart, H. Lin, Unprecedented size-sieving ability in polybenzimidazole doped with polyprotic acids for membrane H_2/CO_2 separation, Energy Environ. Sci. 11 (2018) 94–100.

[45] P. Li, Z. Wang, Z. Qiao, Y. Liu, X. Cao, W. Li, J. Wang, S. Wang, Recent developments in membranes for efficient hydrogen purification, J. Membr. Sci. 495 (2015) 130–168.

[46] D.F. Sanders, Z.P. Smith, R. Guo, L.M. Robeson, J.E. McGrath, D.R. Paul, B.D. Freeman, Energy-efficient polymeric gas separation membranes for a sustainable future: A review, Polymer 54 (2013) 4729–4761.

[47] T. Barbari, W. Koros, D. Paul, Polymeric membranes based on bisphenol-A for gas separations, J. Membr. Sci. 42 (1989) 69–86.

[48] T. Kim, W. Koros, G. Husk, K. O'Brien, Relationship between gas separation properties and chemical structure in a series of aromatic polyimides, J. Membr. Sci. 37 (1988) 45–62.

[49] Y. Maeda, D. Paul, Effect of antiplasticization on selectivity and productivity of gas separation membranes, J. Membr. Sci. 30 (1987) 1–9.

[50] L.M. Robeson, Correlation of separation factor versus permeability for polymeric membranes, J. Membr. Sci. 62 (1991) 165–185.

[51] L.M. Robeson, The upper bound revisited, J. Membr. Sci. 320 (2008) 390–400.

[52] B. Comesaña-Gándara, J. Chen, C.G. Bezzu, M. Carta, I. Rose, M.-C. Ferrari, E. Esposito, A. Fuoco, J.C. Jansen, N.B. McKeown, Redefining the Robeson upper bounds for CO_2/CH_4 and CO_2/N_2 separations using a series of ultrapermeable benzotriptycene-based polymers of intrinsic microporosity, Energy Environ. Sci. 12 (2019) 2733–2740.

[53] B.W. Rowe, L.M. Robeson, B.D. Freeman, D.R. Paul, Influence of temperature on the upper bound: Theoretical considerations and comparison with experimental results, J. Membr. Sci. 360 (2010) 58–69.

[54] Y. Han, W.S.W. Ho, Recent advances in polymeric membranes for CO_2 capture, Chin. J. Chem. Eng. 26 (2018) 2238–2254.

[55] S.R. Reijerkerk, A.C. IJzer, K. Nijmeijer, A. Arun, R.J. Gaymans, M. Wessling, Subambient temperature CO_2 and light gas permeation through segmented block copolymers with tailored soft phase, ACS Appl. Mater. Interfaces 2 (2010) 551–560.

[56] T. Chaubey, S. Kulkarni, D. Hasse, A. Augustine, CO_2 Capture by Cold Membrane Operation with Actual Power Plant Flue Gas, Final Scientific Report, DOE Award Number: DE-FE0013163, 2017. Website: https://doi.org/10.2172/1373105.

[57] D. Hasse, J. Ma, S. Kulkarni, P. Terrien, J.-P. Tranier, E. Sanders, T. Chaubey, J. Brumback, CO_2 capture by cold membrane operation, Energy Procedia 63 (2014) 186–193.

[58] C.H. Lau, P. Li, F. Li, T.-S. Chung, D.R. Paul, Reverse-selective polymeric membranes for gas separations, Prog. Polym. Sci. 38 (2013) 740–766.

[59] J. Park, D. Paul, Correlation and prediction of gas permeability in glassy polymer membrane materials via a modified free volume based group contribution method, J. Membr. Sci. 125 (1997) 23–39.

[60] L.M. Robeson, C.D. Smith, M. Langsam, A group contribution approach to predict permeability and permselectivity of aromatic polymers, J. Membr. Sci. 132 (1997) 33–54.

[61] A. Alentiev, Y. Yampolskii, Correlation of gas permeability and diffusivity with selectivity: Orientations of the clouds of the data points and the effects of temperature, Ind. Eng. Chem. Res. 52 (2013) 8864–8874.

[62] Y. Lou, P. Hao, G. Lipscomb, NELF predictions of a solubility–solubility selectivity upper bound, J. Membr. Sci. 455 (2014) 247–253.

[63] A.Y. Alentiev, Y.P. Yampolskii, Meares equation and the role of cohesion energy density in diffusion in polymers, J. Membr. Sci. 206 (2002) 291–306.

[64] H. Lin, M. Yavari, Upper bound of polymeric membranes for mixed-gas CO_2/CH_4 separations, J. Membr. Sci. 475 (2015) 101–109.

[65] A.Y. Alentiev, Y.P. Yampolskii, Free volume model and tradeoff relations of gas permeability and selectivity in glassy polymers, J. Membr. Sci. 165 (2000) 201–216.

[66] H.B. Park, J. Kamcev, L.M. Robeson, M. Elimelech, B.D. Freeman, Maximizing the right stuff: The trade-off between membrane permeability and selectivity, Science 356 (2017) eaab0530.

[67] J.D. Goddard, J.S. Schultz, S.R. Suchdeo, Facilitated transport via carrier-mediated diffusion in membranes: Part II. Mathematical aspects and analyses, AIChE J. 20 (1974) 625–645.

[68] Y. Han, W.S.W. Ho, Recent advances in polymeric facilitated transport membranes for carbon dioxide separation and hydrogen purification, J. Polym. Sci. 58 (2020) 2435–2449.

[69] R.D. Noble, Analysis of facilitated transport with fixed site carrier membranes, J. Membr. Sci. 50 (1990) 207–214.

[70] P. Danckwerts, The reaction of CO_2 with ethanolamines, Chem. Eng. Sci. 34 (1979) 443–446.

[71] P.V. Kortunov, M. Siskin, L.S. Baugh, D.C. Calabro, In situ nuclear magnetic resonance mechanistic studies of carbon dioxide reactions with liquid amines in aqueous systems: New insights on carbon capture reaction pathways, Energy Fuels 29 (2015) 5919–5939.

[72] Y. Zhao, W.S.W. Ho, Steric hindrance effect on amine demonstrated in solid polymer membranes for CO_2 transport, J. Membr. Sci. 415 (2012) 132–138.

[73] E. Cussler, R. Aris, A. Bhown, On the limits of facilitated diffusion, J. Membr. Sci. 43 (1989) 149–164.

[74] R.D. Noble, Facilitated transport with fixed-site carrier membranes, J. Chem. Soc., Faraday Trans. 87 (1991) 2089–2092.

[75] Y.S. Kang, J.-M. Hong, J. Jang, U.Y. Kim, Analysis of facilitated transport in solid membranes with fixed site carriers 1. Single RC circuit model, J. Membr. Sci. 109 (1996) 149–157.

[76] R. Rea, M.G.D. Angelis, M.G. Baschetti, Models for facilitated transport membranes: A Review, Membranes 9 (2019) 26.

[77] Y. Zhao, W.S.W. Ho, CO_2-selective membranes containing sterically hindered amines for CO_2/H_2 separation, Ind. Eng. Chem. Res. 52 (2012) 8774–8782.

[78] S. Janakiram, M. Ahmadi, Z. Dai, L. Ansaloni, L. Deng, Performance of nanocomposite membranes containing 0D to 2D nanofillers for CO_2 separation: A review, Membranes 8 (2018) 24.

[79] M. Rungta, G.B. Wenz, C. Zhang, L. Xu, W. Qiu, J.S. Adams, W.J. Koros, Carbon molecular sieve structure development and membrane performance relationships, Carbon 115 (2017) 237-248.

[80] L.S. White, X. Wei, S. Pande, T. Wu, T.C. Merkel, Extended flue gas trials with a membrane-based pilot plant at a one-ton-per-day carbon capture rate, J. Membr. Sci. 496 (2015) 48–57.

[81] H. Lin, E. Van Wagner, B.D. Freeman, L.G. Toy, R.P. Gupta, Plasticization-enhanced hydrogen purification using polymeric membranes, Science 311 (2006) 639–642.

[82] H. Lin, B.D. Freeman, Gas and vapor solubility in cross-linked poly(ethylene glycol diacrylate), Macromolecules 38 (2005) 8394–8407.

[83] F. Rindfleisch, T.P. DiNoia, M.A. McHugh, Solubility of polymers and copolymers in supercritical CO_2, J. Phys. Chem. 100 (1996) 15581–15587.

[84] J. Liu, S. Zhang, D. Jiang, C.M. Doherty, A.J. Hill, C. Cheng, H.B. Park, H. Lin, Highly polar but amorphous polymers with robust membrane CO_2/N_2 separation performance, Joule 3 (2019) 1881–1894.

[85] H. Lin, B.D. Freeman, Gas solubility, diffusivity and permeability in poly(ethylene oxide), J. Membr. Sci. 239 (2004) 105–117.

[86] W. Yave, A. Car, S.S. Funari, S.P. Nunes, K.-V. Peinemann, CO_2-philic polymer membrane with extremely high separation performance, Macromolecules 43 (2009) 326–333.

[87] B. Xue, X. Li, L. Gao, M. Gao, Y. Wang, L. Jiang, CO_2-selective free-standing membrane by self-assembly of a UV-crosslinkable diblock copolymer, J. Mater. Chem. 22 (2012) 10918–10923.

[88] W. Yave, H. Huth, A. Car, C. Schick, Peculiarity of a CO_2-philic block copolymer confined in thin films with constrained thickness: “A super membrane for CO_2-capture”, Energy Environ. Sci. 4 (2011) 4656–4661.

[89] S.H. Ahn, S.J. Kim, D.K. Roh, H.-K. Lee, B. Jung, J.H. Kim, Controlling gas permeability of a graft copolymer membrane using solvent vapor treatment, Macromol. Res. 22 (2014) 160–164.

[90] M. Karunakaran, M. Kumar, R. Shevate, F. Akhtar, K.-V. Peinemann, CO_2-philic thin film composite membranes: Synthesis and characterization of PAN-*r*-PEGMA copolymer, Polymers 9 (2017) 219.

[91] F.H. Akhtar, M. Kumar, H. Vovusha, R. Shevate, L.F. Villalobos, U. Schwingenschlögl, K.-V. Peinemann, Scalable synthesis of amphiphilic copolymers for CO_2 -and water-selective

membranes: Effect of copolymer composition and chain length, Macromolecules 52 (2019) 6213–6226.

[92] G.K. Kline, Q. Zhang, J.R. Weidman, R. Guo, PEO-rich semi-interpenetrating polymer network (s-IPN) membranes for CO_2 separation, J. Membr. Sci. 544 (2017) 143–150.

[93] S. Luo, K.A. Stevens, J.S. Park, J.D. Moon, Q. Liu, B.D. Freeman, R. Guo, Highly CO_2-selective gas separation membranes based on segmented copolymers of poly(ethylene oxide) reinforced with pentiptycene-containing polyimide hard segments, ACS Appl. Mater. Interfaces 8 (2016) 2306–2317.

[94] S. Feng, J. Ren, K. Hua, H. Li, X. Ren, M. Deng, Poly(amide-12-*b*-ethylene oxide)/polyethylene glycol blend membranes for carbon dioxide separation, Sep. Purif. Technol. 116 (2013) 25–34.

[95] W. Yave, A. Car, K.-V. Peinemann, Nanostructured membrane material designed for carbon dioxide separation, J. Membr. Sci. 350 (2010) 124–129.

[96] S.R. Reijerkerk, M. Wessling, K. Nijmeijer, Pushing the limits of block copolymer membranes for CO_2 separation, J. Membr. Sci. 378 (2011) 479–484.

[97] N.U. Kim, B.J. Park, M.S. Park, J.T. Park, J.H. Kim, Semi-interpenetrating polymer network membranes based on a self-crosslinkable comb copolymer for CO_2 capture, Chem. Eng. J. 360 (2019) 1468–1476.

[98] Y. Chen, B. Wang, L. Zhao, P. Dutta, W.S.W. Ho, New Pebax®/zeolite Y composite membranes for CO_2 capture from flue gas, J. Membr. Sci. 495 (2015) 415–423.

[99] J.M. Scofield, P.A. Gurr, J. Kim, Q. Fu, S.E. Kentish, G.G. Qiao, Development of novel fluorinated additives for high performance CO_2 separation thin-film composite membranes, J. Membr. Sci. 499 (2016) 191–200.

[100] H. Lin, E. Van Wagner, J.S. Swinnea, B.D. Freeman, S.J. Pas, A.J. Hill, S. Kalakkunnath, D.S. Kalika, Transport and structural characteristics of crosslinked poly(ethylene oxide) rubbers, J. Membr. Sci. 276 (2006) 145–161.

[101] H. Lin, E. Van Wagner, R. Raharjo, B.D. Freeman, I. Roman, High-performance polymer membranes for natural-gas sweetening, Adv. Mater. 18 (2006) 39–44.

[102] V.A. Kusuma, B.D. Freeman, S.L. Smith, A.L. Heilman, D.S. Kalika, Influence of TRIS-based co-monomer on structure and gas transport properties of cross-linked poly(ethylene oxide), J. Membr. Sci. 359 (2010) 25–36.

[103] I. Taniguchi, T. Kai, S. Duan, S. Kazama, H. Jinnai, A compatible crosslinker for enhancement of CO_2 capture of poly(amidoamine) dendrimer-containing polymeric membranes, J. Membr. Sci. 475 (2015) 175–183.

[104] T. Sakaguchi, F. Katsura, A. Iwase, T. Hashimoto, CO_2-permselective membranes of crosslinked poly(vinyl ether)s bearing oxyethylene chains, Polymer 55 (2014) 1459–1466.

[105] S. Quan, S. Li, Z. Wang, X. Yan, Z. Guo, L. Shao, A bio-inspired CO_2-philic network membrane for enhanced sustainable gas separation, J. Mater. Chem. A 3 (2015) 13758–13766.

[106] G.K. Kline, J.R. Weidman, Q. Zhang, R. Guo, Studies of the synergistic effects of crosslink density and crosslink inhomogeneity on crosslinked PEO membranes for CO_2-selective separations, J. Membr. Sci. 544 (2017) 25–34.

[107] J. Xia, S. Liu, T.-S. Chung, Effect of end groups and grafting on the CO_2 separation performance of poly(ethylene glycol) based membranes, Macromolecules 44 (2011) 7727–7736.

[108] S. Li, X. Jiang, X. Yang, Y. Bai, L. Shao, Nanoporous framework “reservoir” maximizing low-molecular-weight enhancer impregnation into CO_2-philic membranes for highly-efficient CO_2 capture, J. Membr. Sci. 570 (2019) 278–285.

[109] A.A. Salih, C. Yi, H. Peng, B. Yang, L. Yin, W. Wang, Interfacially polymerized polyetheramine thin film composite membranes with PDMS inter-layer for CO_2 separation, J. Membr. Sci. 472 (2014) 110–118.

[110] S. Li, Z. Wang, C. Zhang, M. Wang, F. Yuan, J. Wang, S. Wang, Interfacially polymerized thin film composite membranes containing ethylene oxide groups for CO_2 separation, J. Membr. Sci. 436 (2013) 121–131.

[111] J. Liu, G. Zhang, K. Clark, H. Lin, Maximizing ether oxygen content in polymers for membrane CO_2 removal from natural gas, ACS Appl. Mater. Interfaces 11 (2019) 10933–10940.

[112] D.J. Harrigan, J.A. Lawrence, H.W. Reid, J.B. Rivers, J.T. O'Brien, S.A. Sharber, B.J. Sundell, Tunable sour gas separations: Simultaneous H_2S and CO_2 removal from natural gas via crosslinked telechelic poly(ethylene glycol) membranes, J. Membr. Sci. 602 (2020).

[113] L.A. Blanchard, D. Hancu, E.J. Beckman, J.F. Brennecke, Green processing using ionic liquids and CO_2, Nature 399 (1999) 28–29.

[114] P. Scovazzo, J. Kieft, D. Finan, C. Koval, D. Dubois, R. Noble, Gas separations using non-hexafluorophosphate $[PF_6]^-$ anion supported ionic liquid membranes, J. Membr. Sci. 238 (2004) 57–63.

[115] R. Fortunato, C.A.M. Afonso, M.A.M. Reis, J.G. Crespo, Supported liquid membranes using ionic liquids: study of stability and transport mechanisms, J. Membr. Sci. 242 (2004) 197–209.

[116] P. Li, D. Paul, T.-S. Chung, High performance membranes based on ionic liquid polymers for CO_2 separation from the flue gas, Green Chem. 14 (2012) 1052–1063.

[117] J. Grünauer, V. Filiz, S. Shishatskiy, C. Abetz, V. Abetz, Scalable application of thin film coating techniques for supported liquid membranes for gas separation made from ionic liquids, J. Membr. Sci. 518 (2016) 178–191.

[118] M.G. Cowan, D.L. Gin, R.D. Noble, Poly(ionic liquid)/ionic liquid ion-gels with high "free" ionic liquid content: Platform membrane materials for CO_2/light gas separations, Acc. Chem. Res. 49 (2016) 724–732.

[119] S. Kasahara, E. Kamio, A. Yoshizumi, H. Matsuyama, Polymeric ion-gels containing an amino acid ionic liquid for facilitated CO_2 transport media, Chem. Commun. 50 (2014) 2996–2999.

[120] V.A. Kusuma, C. Chen, J.S. Baker, M.K. Macala, D. Hopkinson, The effect of poly(ethylene oxide) cross-linking structure on the mechanical properties and CO_2 separation performance of an ion gel membrane, Polymer 180 (2019) 121666.

[121] J. Deng, J. Yu, Z. Dai, L. Deng, Cross-linked PEG membranes of interpenetrating networks with ILs as additives for enhanced CO_2 separation, Ind. Eng. Chem. Res. 58 (2019) 5261–5268.

[122] V.A. Kusuma, M.K. Macala, J.S. Baker, D. Hopkinson, Cross-linked poly(ethylene oxide) ion gels containing functionalized imidazolium ionic liquids as carbon dioxide separation membranes, Ind. Eng. Chem. Res. 57 (2018) 11658–11667.

[123] K. Kodama, R. Tsuda, K. Niitsuma, T. Tamura, T. Ueki, H. Kokubo, M. Watanabe, Structural effects of polyethers and ionic liquids in their binary mixtures on lower critical solution temperature liquid-liquid phase separation, Polym. J. 43 (2011) 242–248.

[124] V.A. Kusuma, M.K. Macala, J. Liu, A.M. Marti, R.J. Hirsch, L.J. Hill, D. Hopkinson, Ionic liquid compatibility in polyethylene oxide/siloxane ion gel membranes, J. Membr. Sci. 545 (2018) 292–300.

[125] A. Klemm, Y.-Y. Lee, H. Mao, B. Gurkan, Facilitated transport membranes with ionic liquids for CO_2 separations, Front. Chem. 8 (2020) 637.

[126] Z. Dai, R.D. Noble, D.L. Gin, X. Zhang, L. Deng, Combination of ionic liquids with membrane technology: A new approach for CO_2 separation, J. Membr. Sci. 497 (2016) 1–20.

[127] I. Kammakakam, K.E. O'Harra, J.E. Bara, E.M. Jackson, Design and synthesis of imidazolium-mediated Tröger's base-containing ionene polymers for advanced CO_2 separation membranes, ACS Omega 4 (2019) 3439–3448.

[128] M.S. Mittenthal, B.S. Flowers, J.E. Bara, J.W. Whitley, S.K. Spear, J.D. Roveda, D.A. Wallace, M.S. Shannon, R. Holler, R. Martens, Ionic polyimides: Hybrid polymer architectures and composites with ionic liquids for advanced gas separation membranes, Ind. Eng. Chem. Res. 56 (2017) 5055–5069.

[129] J. Yin, C. Zhang, Y. Yu, T. Hao, H. Wang, X. Ding, J. Meng, Tuning the microstructure of crosslinked poly(ionic liquid) membranes and gels via a multicomponent reaction for improved CO_2 capture performance, J. Membr. Sci. 593 (2020) 117405.

[130] A. Ito, T. Yasuda, T. Yoshioka, A. Yoshida, X. Li, K. Hashimoto, K. Nagai, M. Shibayama, M. Watanabe, Sulfonated polyimide/ionic liquid composite membranes for CO_2 separation: transport properties in relation to their nanostructures, Macromolecules 51 (2018) 7112–7120.

[131] L.C. Tomé, D.C. Guerreiro, R.M. Teodoro, V.D. Alves, I.M. Marrucho, Effect of polymer molecular weight on the physical properties and CO_2/N_2 separation of pyrrolidinium-based poly(ionic liquid) membranes, J. Membr. Sci. 549 (2018) 267–274.

[132] R.M. Teodoro, L.C. Tomé, D. Mantione, D. Mecerreyes, I.M. Marrucho, Mixing poly(ionic liquid)s and ionic liquids with different cyano anions: Membrane forming ability and CO_2/N_2 separation properties, J. Membr. Sci. 552 (2018) 341–348.

[133] T.C. Merkel, I. Pinnau, R. Prabhakar, B.D. Freeman, Gas and Vapor Transport Properties of Perfluoropolymers, in: B.D. Freeman, Y. Yampolskii, I. Pinnau (Eds.) Material Science of Membranes for Gas and Vapor Separation, John Wiley & Sons, 2006.

[134] Y. Okamoto, H.-C. Chiang, M. Fang, M. Galizia, T. Merkel, M. Yavari, H. Nguyen, H. Lin, Perfluorodioxolane polymers for gas separation membrane applications, Membranes 10 (2020) 394.

[135] J. Scheirs, Modern fluoropolymers: High performance polymers for diverse applications, Wiley, New York, NY, 1997.

[136] I. Pinnau, L.G. Toy, Gas and vapor transport properties of amorphous perfluorinated copolymer membranes based on 2,2-bistrifluoromethyl-4,5-difluoro-1,3-dioxole/tetrafluoroethylene, J. Membr. Sci. 109 (1996) 125–133.

[137] T. Merkel, V. Bondar, K. Nagai, B. Freeman, Y.P. Yampolskii, Gas sorption, diffusion, and permeation in poly(2,2-bis(trifluoromethyl)-4,5-difluoro-1,3-dioxole-*co*-tetrafluoroethylene), Macromolecules 32 (1999) 8427–8440.

[138] M. Fang, Y. Okamoto, Y. Koike, Z. He, T.C. Merkel, Gas separation membranes prepared with copolymers of perfluoro(2-methylene-4,5-dimethyl-1,3-dioxlane) and chlorotrifluoroethylene, J. Fluorine Chem. 188 (2016) 18–22.

[139] Y. Okamoto, H. Zhang, F. Mikes, Y. Koike, Z. He, T.C. Merkel, New perfluoro-dioxolane-based membranes for gas separations, J. Membr. Sci. 471 (2014) 412–419.

[140] M. Yavari, M. Fang, H. Nguyen, T.C. Merkel, H. Lin, Y. Okamoto, Dioxolane-based perfluoropolymers with superior membrane gas separation properties, Macromolecules 51 (2018) 2489–2497.

[141] N.A. Belov, R.Y. Nikiforov, M.V. Bermeshev, Y.P. Yampolskii, E.S. Finkelshtein, Synthesis and gas transport properties of polypentafluorostyrene, Pet. Chem. 57 (2017) 923–928.

[142] M. Fang, Z. He, T.C. Merkel, Y. Okamoto, High-performance perfluorodioxolane copolymer membranes for gas separation with tailored selectivity enhancement, J. Mater. Chem. A 6 (2018) 652–658.

[143] H.-C. Chiang, M. Fang, Y. Okamoto, Mechanical, optical and gas transport properties of poly(perfluoro-2-methylene-4-methyl-1,3-dioxolane) membrane containing perfluoropolyether as a plasticizer, J. Fluorine Chem. 236 (2020) 109572.

[144] R.R. Tiwari, Z.P. Smith, H. Lin, B. Freeman, D. Paul, Gas permeation in thin films of "high free-volume" glassy perfluoropolymers: Part I. Physical aging, Polymer 55 (2014) 5788–5800.

[145] R.R. Tiwari, Z.P. Smith, H. Lin, B. Freeman, D. Paul, Gas permeation in thin films of "high free-volume" glassy perfluoropolymers: Part II. CO_2 plasticization and sorption, Polymer 61 (2015) 1–14.

[146] M. Yavari, T. Le, H. Lin, Physical aging of glassy perfluoropolymers in thin film composite membranes. Part I. Gas transport properties, J. Membr. Sci. 525 (2017) 387–398.

[147] M. Yavari, S. Maruf, Y. Ding, H. Lin, Physical aging of glassy perfluoropolymers in thin film composite membranes. Part II. Glass transition temperature and the free volume model, J. Membr. Sci. 525 (2017) 399–408.

[148] H.B. Park, C.H. Jung, Y.M. Lee, A.J. Hill, S.J. Pas, S.T. Mudie, E. Van Wagner, B.D. Freeman, D.J. Cookson, Polymers with cavities tuned for fast selective transport of small molecules and ions, Science 318 (2007) 254–258.

[149] S.H. Han, N. Misdan, S. Kim, C.M. Doherty, A.J. Hill, Y.M. Lee, Thermally rearranged (TR) polybenzoxazole: Effects of diverse imidization routes on physical properties and gas transport behaviors, Macromolecules 43 (2010) 7657–7667.

[150] C. Aguilar-Lugo, C. Álvarez, Y.M. Lee, J.G. de la Campa, A.n.E. Lozano, Thermally rearranged polybenzoxazoles containing bulky adamantyl groups from *ortho*-substituted precursor copolyimides, Macromolecules 51 (2018) 1605–1619.

[151] R. Guo, D.F. Sanders, Z.P. Smith, B.D. Freeman, D.R. Paul, J.E. McGrath, Synthesis and characterization of thermally rearranged (TR) polymers: Effect of glass transition temperature of aromatic poly (hydroxyimide) precursors on TR process and gas permeation properties, J. Mater. Chem. A 1 (2013) 6063–6072.

[152] C.H. Park, E. Tocci, Y.M. Lee, E. Drioli, Thermal treatment effect on the structure and property change between hydroxy-containing polyimides (HPIs) and thermally rearranged polybenzoxazole (TR-PBO), J. Phys. Chem. B 116 (2012) 12864−12877.

[153] L. Ye, L. Wang, X. Jie, C. Yu, G. Kang, Y. Cao, The evolution of free volume and gas transport properties for the thermal rearrangement of poly(hydroxyamide-*co*-amide)s membranes, J. Membr. Sci. 573 (2019) 21–35.

[154] S.H. Han, J.E. Lee, K.-J. Lee, H.B. Park, Y.M. Lee, Highly gas permeable and microporous polybenzimidazole membrane by thermal rearrangement, J. Membr. Sci. 357 (2010) 143–151.

[155] A. Murugesan, S. Sivaram, Understanding structure and composition of thermally rearranged polymers based on small‐molecule chemistry: A perspective, Polym. Int. 68 (2019) 1649–1661.

[156] D.F. Sanders, Z.P. Smith, C.P. Ribeiro, R. Guo, J.E. McGrath, D.R. Paul, B.D. Freeman, Gas permeability, diffusivity, and free volume of thermally rearranged polymers based on 3,3′-dihydroxy-4,4′-diamino-biphenyl (HAB) and 2,2′-bis-(3,4-dicarboxyphenyl) hexafluoropropane dianhydride (6FDA), J. Membr. Sci. 409–410 (2012) 232–241.

[157] Z.P. Smith, D.F. Sanders, C.P. Ribeiro, R. Guo, B.D. Freeman, D.R. Paul, J.E. McGrath, S. Swinnea, Gas sorption and characterization of thermally rearranged polyimides based on 3,3′-dihydroxy-4,4′-diamino-biphenyl (HAB) and 2,2′-bis-(3,4-dicarboxyphenyl) hexafluoropropane dianhydride (6FDA), J. Membr. Sci. 415–416 (2012) 558–567.

[158] Z.P. Smith, R.R. Tiwari, T.M. Murphy, D.F. Sanders, K.L. Gleason, D.R. Paul, B.D. Freeman, Hydrogen sorption in polymers for membrane applications, Polymer 54 (2013) 3026–3037.

[159] S. Kim, S.H. Han, Y.M. Lee, Thermally rearranged (TR) polybenzoxazole hollow fiber membranes for CO_2 capture, J. Membr. Sci. 403 (2012) 169–178.

[160] K.T. Woo, J. Lee, G. Dong, J.S. Kim, Y.S. Do, W.-S. Hung, K.-R. Lee, G. Barbieri, E. Drioli, Y.M. Lee, Fabrication of thermally rearranged (TR) polybenzoxazole hollow fiber membranes with superior CO_2/N_2 separation performance, J. Membr. Sci. 490 (2015) 129–138.

[161] G. Tullos, L. Mathias, Unexpected thermal conversion of hydroxy-containing polyimides to polybenzoxazoles, Polymer 40 (1999) 3463–3468.

[162] H. Wang, T.-S. Chung, The evolution of physicochemical and gas transport properties of thermally rearranged polyhydroxyamide (PHA), J. Membr. Sci. 385 (2011) 86–95.

[163] Z.P. Smith, G. Hernández, K.L. Gleason, A. Anand, C.M. Doherty, K. Konstas, C. Alvarez, A.J. Hill, A.E. Lozano, D.R. Paul, B.D. Freeman, Effect of polymer structure on gas transport properties of selected aromatic polyimides, polyamides and TR polymers, J. Membr. Sci. 493 (2015) 766–781.

[164] Z.-X. Low, P.M. Budd, N.B. McKeown, D.A. Patterson, Gas Permeation Properties, Physical Aging, and Its Mitigation in High Free Volume Glassy Polymers, Chem. Rev. 118 (2018) 5871–5911.

[165] B. Comesaña-Gandara, L. Ansaloni, Y.M. Lee, A.E. Lozano, M.G. De Angelis, Sorption, diffusion, and permeability of humid gases and aging of thermally rearranged (TR) polymer membranes from a novel ortho-hydroxypolyimide, J. Membr. Sci. 542 (2017) 439–455.

[166] A. Brunetti, M. Cersosimo, G. Dong, K.T. Woo, J. Lee, J.S. Kim, Y.M. Lee, E. Drioli, G. Barbieri, In situ restoring of aged thermally rearranged gas separation membranes, J. Membr. Sci. 520 (2016) 671–678.

[167] M. Calle, C.M. Doherty, A.J. Hill, Y.M. Lee, Cross-linked thermally rearranged poly (benzoxazole-*co*-imide) membranes for gas separation, Macromolecules 46 (2013) 8179–8189.

[168] M. Calle, H.J. Jo, C.M. Doherty, A.J. Hill, Y.M. Lee, Cross-linked thermally rearranged poly (benzoxazole-*co*-imide) membranes prepared from *ortho*-hydroxycopolyimides containing pendant carboxyl groups and gas separation properties, Macromolecules 48 (2015) 2603–2613.

[169] J. Lee, J.S. Kim, J.F. Kim, H.J. Jo, H. Park, J.G. Seong, Y.M. Lee, Densification-induced hollow fiber membranes using crosslinked thermally rearranged (XTR) polymer for CO_2 capture, J. Membr. Sci. 573 (2019) 393–402.

[170] J. Lee, J.S. Kim, S.-y. Moon, C.Y. Park, J.F. Kim, Y.M. Lee, Dimensionally-controlled densification in crosslinked thermally rearranged (XTR) hollow fiber membranes for CO_2 capture, J. Membr. Sci. 595 (2020) 117535.

[171] H.J. Jo, C.Y. Soo, G. Dong, Y.S. Do, H.H. Wang, M.J. Lee, J.R. Quay, M.K. Murphy, Y.M. Lee, Thermally rearranged poly (benzoxazole-*co*-imide) membranes with superior mechanical strength for gas separation obtained by tuning chain rigidity, Macromolecules 48 (2015) 2194–2202.

[172] C.A. Scholes, C.P. Ribeiro, S.E. Kentish, B.D. Freeman, Thermal rearranged poly (benzoxazole-*co*-imide) membranes for CO_2 separation, J. Membr. Sci. 450 (2014) 72–80.

[173] J.I. Choi, C.H. Jung, S.H. Han, H.B. Park, Y.M. Lee, Thermally rearranged (TR) poly (benzoxazole-*co*-pyrrolone) membranes tuned for high gas permeability and selectivity, J. Membr. Sci. 349 (2010) 358–368.

[174] Y.F. Yeong, H. Wang, K. Pallathadka Pramoda, T.-S. Chung, Thermal induced structural rearrangement of cardo-copolybenzoxazole membranes for enhanced gas transport properties, J. Membr. Sci. 397–398 (2012) 51–65.

[175] S. Li, H.J. Jo, S.H. Han, C.H. Park, S. Kim, P.M. Budd, Y.M. Lee, Mechanically robust thermally rearranged (TR) polymer membranes with spirobisindane for gas separation, J. Membr. Sci. 434 (2013) 137–147.

[176] X. Hu, W.H. Lee, J.Y. Bae, J.S. Kim, J.T. Jung, H.H. Wang, H.J. Park, Y.M. Lee, Thermally rearranged polybenzoxazole copolymers incorporating Tröger's base for high flux gas separation membranes, J. Membr. Sci. 612 (2020) 118437.

[177] L. Ye, X. Jie, L. Wang, G. Xu, Y. Sun, G. Kang, Y. Cao, Preparation and gas separation performance of thermally rearranged poly(benzoxazole-*co*-amide) (TR-PBOA) hollow fiber membranes deriving from polyamides, Sep. Purif. Technol. 257 (2021) 117870.

[178] K.T. Woo, J. Lee, G. Dong, J.S. Kim, Y.S. Do, H.J. Jo, Y.M. Lee, Thermally rearranged poly(benzoxazole-*co*-imide) hollow fiber membranes for CO_2 capture, J. Membr. Sci. 498 (2016) 125–134.

[179] K.T. Woo, G. Dong, J. Lee, J.S. Kim, Y.S. Do, W.H. Lee, H.S. Lee, Y.M. Lee, Ternary mixed-gas separation for flue gas CO_2 capture using high performance thermally rearranged (TR) hollow fiber membranes, J. Membr. Sci. 510 (2016) 472–480.

[180] Y. Jiang, C.F. Chen, Recent developments in synthesis and applications of triptycene and pentiptycene derivatives, Eur. J. Org. Chem. 2011 (2011) 6377–6403.

[181] M. Mastalerz, S. Sieste, M. Cenic, I.M. Oppel, Two-step synthesis of hexaammonium triptycene: An air-stable building block for condensation reactions to extended triptycene derivatives, J. Org. Chem. 76 (2011) 6389–6393.

[182] F. Alghunaimi, B. Ghanem, N. Alaslai, R. Swaidan, E. Litwiller, I. Pinnau, Gas permeation and physical aging properties of iptycene diamine-based microporous polyimides, J. Membr. Sci. 490 (2015) 321–327.

[183] S. Luo, J.R. Wiegand, P. Gao, C.M. Doherty, A.J. Hill, R. Guo, Molecular origins of fast and selective gas transport in pentiptycene-containing polyimide membranes and their physical aging behavior, J. Membr. Sci. 518 (2016) 100–109.

[184] T.M. Long, T.M. Swager, Using “internal free volume” to increase chromophore alignment, J. Am. Chem. Soc. 124 (2002) 3826–3827.

[185] J.R. Weidman, R. Guo, The use of iptycenes in rational macromolecular design for gas separation membrane applications, Ind. Eng. Chem. Res. 56 (2017) 4220–4236.

[186] Y.J. Cho, H.B. Park, High performance polyimide with high internal free volume elements, Macromol. Rapid Commun. 32 (2011) 579–586.

[187] S. Luo, Q. Liu, B. Zhang, J.R. Wiegand, B.D. Freeman, R. Guo, Pentiptycene-based polyimides with hierarchically controlled molecular cavity architecture for efficient membrane gas separation, J. Membr. Sci. 480 (2015) 20–30.

[188] S. Luo, J.R. Wiegand, B. Kazanowska, C.M. Doherty, K. Konstas, A.J. Hill, R. Guo, Finely tuning the free volume architecture in iptycene-containing polyimides for highly selective and fast hydrogen transport, Macromolecules 49 (2016) 3395–3405.

[189] S. Luo, J. Liu, H. Lin, B.A. Kazanowska, M.D. Hunckler, R.K. Roeder, R. Guo, Preparation and gas transport properties of triptycene-containing polybenzoxazole (PBO)-based polymers derived from thermal rearrangement (TR) and thermal cyclodehydration (TC) processes, J. Mater. Chem. A 4 (2016) 17050–17062.

[190] S. Luo, Q. Zhang, T.K. Bear, T.E. Curtis, R.K. Roeder, C.M. Doherty, A.J. Hill, R. Guo, Triptycene-containing poly(benzoxazole-*co*-imide) membranes with enhanced mechanical strength for high-performance gas separation, J. Membr. Sci. 551 (2018) 305–314.

[191] S. Luo, Q. Zhang, L. Zhu, H. Lin, B.A. Kazanowska, C.M. Doherty, A.J. Hill, P. Gao, R. Guo, Highly selective and permeable microporous polymer membranes for hydrogen purification and CO_2 removal from natural gas, Chem. Mater. 30 (2018) 5322–5332.

[192] R.D. Crist, Z. Huang, R. Guo, M. Galizia, Effect of thermal treatment on the structure and gas transport properties of a triptycene-based polybenzoxazole exhibiting configurational free volume, J. Membr. Sci. 597 (2020).

[193] V. Loianno, S. Luo, Q. Zhang, R. Guo, M. Galizia, Gas and water vapor sorption and diffusion in a triptycene-based polybenzoxazole: Effect of temperature and pressure and predicting of mixed gas sorption, J. Membr. Sci. 574 (2019) 100–111.

[194] B.S. Ghanem, R. Swaidan, E. Litwiller, I. Pinnau, Ultra-microporous triptycene-based polyimide membranes for high-performance gas separation, Adv. Mater. 26 (2014) 3688–3692.

[195] R. Swaidan, M. Al-Saeedi, B. Ghanem, E. Litwiller, I. Pinnau, Rational design of intrinsically ultramicroporous polyimides containing bridgehead-substituted triptycene for highly selective and permeable gas separation membranes, Macromolecules 47 (2014) 5104–5114.

[196] R. Swaidan, B. Ghanem, E. Litwiller, I. Pinnau, Effects of hydroxyl-functionalization and sub-T_g thermal annealing on high pressure pure- and mixed-gas CO_2/CH_4 separation by polyimide membranes based on 6FDA and triptycene-containing dianhydrides, J. Membr. Sci. 475 (2015) 571–581.

[197] H. Mao, S. Zhang, Synthesis, characterization, and gas transport properties of novel iptycene-based poly[bis(benzimidazobenzisoquinolinones)], Polymer 55 (2014) 102–109.

[198] B.S. Ghanem, R. Swaidan, X. Ma, E. Litwiller, I. Pinnau, Energy‐efficient hydrogen separation by AB‐type ladder‐polymer molecular sieves, Adv. Mater. 26 (2014) 6696‐6700.

[199] I. Rose, M. Carta, R. Malpass-Evans, M.-C. Ferrari, P. Bernardo, G. Clarizia, J.C. Jansen, N.B. McKeown, Highly permeable benzotriptycene-based polymer of intrinsic microporosity, ACS Macro Letters 4 (2015) 912–915.

[200] J.D. Moon, A.T. Bridge, C. D'Ambra, B.D. Freeman, D.R. Paul, Gas separation properties of polybenzimidazole/thermally-rearranged polymer blends, J. Membr. Sci. (2019).

[201] J.D. Moon, M. Galizia, H. Borjigin, R. Liu, J.S. Riffle, B.D. Freeman, D.R. Paul, Modeling water diffusion in polybenzimidazole membranes using partial immobilization and free volume theory, Polymer (2020) 122170.

[202] J.D. Moon, M. Galizia, H. Borjigin, R. Liu, J.S. Riffle, B.D. Freeman, D.R. Paul, Water vapor sorption, diffusion, and dilation in polybenzimidazoles, Macromolecules 51 (2018) 7197–7208.

[203] K.A. Stevens, J.D. Moon, H. Borjigin, R. Liu, R.M. Joseph, J.S. Riffle, B.D. Freeman, Influence of temperature on gas transport properties of tetraaminodiphenylsulfone (TADPS) based polybenzimidazoles, J. Membr. Sci. 593 (2020).

[204] L. Zhu, M.T. Swihart, H. Lin, Tightening polybenzimidazole (PBI) nanostructure via chemical cross-linking for membrane H_2/CO_2 separation, J. Mater. Chem. A 5 (2017) 19914–19923.

[205] Z. Ali, F. Pacheco, E. Litwiller, Y. Wang, Y. Han, I. Pinnau, Ultra-selective defect-free interfacially polymerized molecular sieve thin-film composite membranes for H_2 purification, J. Mater. Chem. A 6 (2018) 30–35.

[206] V.A. Kusuma, J.S. McNally, J.S. Baker, Z. Tong, L. Zhu, C.J. Orme, F.F. Stewart, D.P. Hopkinson, Cross-linked polyphosphazene blends as robust CO_2 separation membranes, ACS Appl. Mater. Interfaces 12 (2020) 30787–30795.

[207] C.R. Maroon, J. Townsend, K.R. Gmernicki, D.J. Harrigan, B.J. Sundell, J.A. Lawrence III, S.M. Mahurin, K.D. Vogiatzis, B.K. Long, Elimination of CO_2/N_2 Langmuir Sorption and Promotion of "N_2-Phobicity" within High-T_g Glassy Membranes, Macromolecules 52 (2019) 1589–1600.

[208] S.A. Lawrence, Amines: Synthesis, Properties and Applications, Cambridge University Press, Cambridge, United Kingdom, 2004.

[209] T.J. Kim, B. Li, M.B. Hägg, Novel fixed-site-carrier polyvinylamine membrane for carbon dioxide capture, J. Polym. Sci. Part B: Polym. Phys. 42 (2004) 4326–4336.

[210] S.B. Hamouda, Q.T. Nguyen, D. Langevin, S. Roudesli, Poly(vinylalcohol)/poly(ethyleneglycol)/poly(ethyleneimine) blend membranes-structure and CO_2 facilitated transport, C. R. Chim. 13 (2010) 372–379.

[211] S. Duan, I. Taniguchi, T. Kai, S. Kazama, Poly(amidoamine) dendrimer/poly(vinyl alcohol) hybrid membranes for CO_2 capture, J. Membr. Sci. 423–424 (2012) 107–112.

[212] Y. Liu, S. Yu, H. Wu, Y. Li, S. Wang, Z. Tian, Z. Jiang, High permeability hydrogel membranes of chitosan/polyether-block-amide blends for CO_2 separation, J. Membr. Sci. 469 (2014) 198–208.

[213] B. Prasad, B. Mandal, Moisture responsive and CO_2 selective biopolymer membrane containing silk fibroin as a green carrier for facilitated transport of CO_2, J. Membr. Sci. 550 (2018) 416–426.

[214] B. Prasad, R.M. Thakur, B. Mandal, B. Su, Enhanced CO_2 separation membrane prepared from waste by-product of silk fibroin, J. Membr. Sci. 587 (2019) 117170.

[215] M.S.A. Rahaman, L. Zhang, L.-H. Cheng, X.-H. Xu, H.-L. Chen, Capturing carbon dioxide from air using a fixed carrier facilitated transport membrane, RSC Adv. 2 (2012) 9165–9172.

[216] I. Taniguchi, S. Duan, T. Kai, S. Kazama, H. Jinnai, Effect of the phase-separated structure on CO_2 separation performance of the poly(amidoamine) dendrimer immobilized in a poly(ethylene glycol) network, J. Mater. Chem. A 1 (2013) 14514–14523.

[217] R. Pelton, Polyvinylamine: A tool for engineering interfaces, Langmuir 30 (2014) 15373–15382.

[218] Y. Chen, W.S.W. Ho, High-molecular-weight polyvinylamine/piperazine glycinate membranes for CO_2 capture from flue gas, J. Membr. Sci. 514 (2016) 376–384.

[219] M. Sandru, T.-J. Kim, M.-B. Hägg, High molecular fixed-site-carrier PVAm membrane for CO_2 capture, Desalination 240 (2009) 298–300.

[220] M. Sandru, S.H. Haukebø, M.-B. Hägg, Composite hollow fiber membranes for CO_2 capture, J. Membr. Sci. 346 (2010) 172–186.

[221] L. Deng, M.-B. Hägg, Fabrication and evaluation of a blend facilitated transport membrane for CO_2/CH_4 separation, Ind. Eng. Chem. Res. 54 (2015) 11139–11150.

[222] D. Wu, Y. Han, W. Salim, K.K. Chen, J. Li, W.S.W. Ho, Hydrophilic and morphological modification of nanoporous polyethersulfone substrates for composite membranes in CO_2 separation, J. Membr. Sci. 565 (2018) 439–449.

[223] D. Wu, L. Zhao, V.K. Vakharia, W. Salim, W.S.W. Ho, Synthesis and characterization of nanoporous polyethersulfone membrane as support for composite membrane in CO_2 separation: From lab to pilot scale, J. Membr. Sci. 510 (2016) 58–71.

[224] R. Pang, K.K. Chen, Y. Han, W.S.W. Ho, Highly permeable polyethersulfone substrates with bicontinuous structure for composite membranes in CO_2/N_2 separation, J. Membr. Sci. 612 (2020) 118443.

[225] P. Li, Z. Wang, W. Li, Y. Liu, J. Wang, S. Wang, High-performance multilayer composite membranes with mussel-inspired polydopamine as a versatile molecular bridge for CO_2 separation, ACS Appl. Mater. Interfaces 7 (2015) 15481–15493.

[226] Z. Qiao, S. Zhao, M. Sheng, J. Wang, S. Wang, Z. Wang, C. Zhong, M.D. Guiver, Metal-induced ordered microporous polymers for fabricating large-area gas separation membranes, Nat. Mater. (2018) 1.

[227] S. Dong, Z. Wang, M. Sheng, Z. Qiao, J. Wang, High-performance multi-layer composite membrane with enhanced interlayer compatibility and surface crosslinking for CO_2 separation, J. Membr. Sci. 610 (2020) 118221.

[228] P.V. Kortunov, M. Siskin, M. Paccagnini, H. Thomann, CO_2 reaction mechanisms with hindered alkanolamines: Control and promotion of reaction pathways, Energy Fuels 30 (2016) 1223–1236.

[229] G. Sartori, D.W. Savage, Sterically hindered amines for carbon dioxide removal from gases, Ind. Eng. Chem. Fundam. 22 (1983) 239–249.

[230] Z. Tong, W.S.W. Ho, New sterically hindered polyvinylamine membranes for CO_2 separation and capture, J. Membr. Sci. 543 (2017) 202–211.

[231] S. Li, Z. Wang, X. Yu, J. Wang, S. Wang, High-performance membranes with multi-permselectivity for CO_2 separation, Adv. Mater. 24 (2012) 3196–3200.

[232] W. He, Z. Wang, W. Li, S. Li, Z. Bai, J. Wang, S. Wang, Cyclic tertiary amino group containing fixed carrier membranes for CO_2 separation, J. Membr. Sci. 476 (2015) 171–181.

[233] X. Yu, Z. Wang, Z. Wei, S. Yuan, J. Zhao, J. Wang, S. Wang, Novel tertiary amino containing thin film composite membranes prepared by interfacial polymerization for CO_2 capture, J. Membr. Sci. 362 (2010) 265–278.

[234] W.S.W. Ho, Membranes Comprising Salts of Aminoacids in Hydrophilic Polymers, U. S. Patent 5,611,843 (1997)

[235] W.S.W. Ho, Membranes Comprising Aminoacid Salts in Polyamine Polymers and Blends, U. S. Patent 6,099,621 (2000)

[236] H. Bai, W.S.W. Ho, New carbon dioxide-selective membranes based on sulfonated polybenzimidazole (SPBI) copolymer matrix for fuel cell applications, Ind. Eng. Chem. Res. 48 (2008) 2344–2354.

[237] Y. Chen, L. Zhao, B. Wang, P. Dutta, W.S.W. Ho, Amine-containing polymer/zeolite Y composite membranes for CO_2/N_2 separation, J. Membr. Sci. 497 (2016) 21–28.

[238] Y. Han, D. Wu, W.S.W. Ho, Nanotube-reinforced facilitated transport membrane for CO_2/N_2 separation with vacuum operation, J. Membr. Sci. 567 (2018) 261–271.

[239] Y. Han, D. Wu, W.S.W. Ho, Simultaneous effects of temperature and vacuum and feed pressures on facilitated transport membrane for CO_2/N_2 separation, J. Membr. Sci. 573 (2019) 476–484.

[240] J. Zou, W.S.W. Ho, CO_2-selective polymeric membranes containing amines in crosslinked poly(vinyl alcohol), J. Membr. Sci. 286 (2006) 310–321.

[241] X. Deng, C. Zou, Y. Han, L.-C. Lin, W.S.W. Ho, Computational evaluation of carriers in facilitated transport membranes for postcombustion carbon capture, J. Phys. Chem. C 124 (2020) 25322–25330.

[242] W. Salim, Y. Han, V. Vakharia, D. Wu, D.J. Wheeler, W.S.W. Ho, Scale-up of amine-containing membranes for hydrogen purification for fuel cells, J. Membr. Sci. 573 (2019) 465–475.

[243] V. Vakharia, W. Salim, D. Wu, Y. Han, Y. Chen, L. Zhao, W.S.W. Ho, Scale-up of amine-containing thin-film composite membranes for CO_2 capture from flue gas, J. Membr. Sci. 555 (2018) 379–387.

[244] D. Wu, Y. Han, L. Zhao, W. Salim, V. Vakharia, W.S.W. Ho, Scale-up of zeolite-Y/polyethersulfone substrate for composite membrane fabrication in CO_2 separation, J. Membr. Sci. 562 (2018) 56–66.

[245] W. Salim, V. Vakharia, Y. Chen, D. Wu, Y. Han, W.S.W. Ho, Fabrication and field testing of spiral-wound membrane modules for CO_2 capture from flue gas, J. Membr. Sci. 556 (2018) 126–137.

[246] K.K. Chen, W. Salim, Y. Han, D. Wu, W.S.W. Ho, Fabrication and scale-up of multi-leaf spiral-wound membrane modules for CO_2 capture from flue gas, J. Membr. Sci. 595 (2020) 117504.

[247] Y. Han, W. Salim, K.K. Chen, D. Wu, W.S.W. Ho, Field trial of spiral-wound facilitated transport membrane module for CO_2 capture from flue gas, J. Membr. Sci. 575 (2019) 242–251.

[248] S. Yuan, Z. Wang, Z. Qiao, M. Wang, J. Wang, S. Wang, Improvement of CO_2/N_2 separation characteristics of polyvinylamine by modifying with ethylenediamine, J. Membr. Sci. 378 (2011) 425–437.

[249] Z. Qiao, Z. Wang, S. Yuan, J. Wang, S. Wang, Preparation and characterization of small molecular amine modified PVAm membranes for CO_2/H_2 separation, J. Membr. Sci. 475 (2015) 290–302.

[250] Z. Dai, J. Deng, L. Ansaloni, S. Janakiram, L. Deng, Thin-film-composite hollow fiber membranes containing amino acid salts as mobile carriers for CO2 separation, J. Membr. Sci. 578 (2019) 61–68.

[251] S. Janakiram, X. Yu, L. Ansaloni, Z. Dai, L. Deng, Manipulation of fibril surfaces in nanocellulose-based hybrid facilitated transport membranes for enhanced CO_2 capture, ACS Appl. Mater. Interfaces 11 (2019) 33302–33313.

[252] J.S. Schultz, J.D. Goddard, S.R. Suchdeo, Facilitated transport via carrier-mediated diffusion in membranes: Part I. Mechanistic aspects, experimental systems and characteristic regimes, AIChE J. 20 (1974) 417–445.

[253] Y. Han, W.S.W. Ho, Design of amine-containing CO_2-selective membrane process for carbon capture from flue gas, Ind. Eng. Chem. Res. 59 (2020) 5340–5350.

[254] L. Ansaloni, Y. Zhao, B.T. Jung, K. Ramasubramanian, M.G. Baschetti, W.S.W. Ho, Facilitated transport membranes containing amino-functionalized multi-walled carbon nanotubes for high-pressure CO_2 separations, J. Membr. Sci. 490 (2015) 18–28.

[255] W.S.W. Ho, D. Dalrymple, Facilitated transport of olefins in Ag^+-containing polymer membranes, J. Membr. Sci. 91 (1994) 13–25.

[256] R.D. Noble, J.D. Way, L.A. Powers, Effect of external mass-transfer resistance on facilitated transport, Ind. Eng. Chem. Fundam. 25 (1986) 450–452.

[257] B. Belaissaoui, E. Lasseuguette, S. Janakiram, L. Deng, M.C. Ferrari, Analysis of CO_2 facilitation transport effect through a hybrid poly(allyl amine) membrane: Pathways for further improvement, Membranes 10 (2020) 367.

[258] K.K. Chen, Y. Han, Z. Tong, M. Gasda, W.S.W. Ho, Membrane processes for CO_2 removal and fuel utilization enhancement for solid oxide fuel cells, J. Membr. Sci. 620 (2020) 118846.

[259] A. Sayari, A. Heydari-Gorji, Y. Yang, CO_2-induced degradation of amine-containing adsorbents: Reaction products and pathways, J. Am. Chem. Soc. 134 (2012) 13834–13842.

[260] C. Gouedard, D. Picq, F. Launay, P.-L. Carrette, Amine degradation in CO_2 capture. I. A review, Int. J. Greenh. Gas Con. 10 (2012) 244–270.

[261] A. Heydari-Gorji, Y. Belmabkhout, A. Sayari, Degradation of amine-supported CO_2 adsorbents in the presence of oxygen-containing gases, Microporous Mesoporous Mater. 145 (2011) 146–149.

[262] V. Vakharia, W. Salim, M. Gasda, W.S.W. Ho, Oxidatively stable membranes for CO_2 separation and H_2 purification, J. Membr. Sci. 533 (2017) 220–228.

[263] W. Salim, V. Vakharia, K.K. Chen, M. Gasda, W.S.W. Ho, Oxidatively stable borate-containing membranes for H_2 purification for fuel cells, J. Membr. Sci. 562 (2018) 9–17.

[264] S. Chempath, J.M. Boncella, L.R. Pratt, N. Henson, B.S. Pivovar, Density functional theory study of degradation of tetraalkylammonium hydroxides, J. Phys. Chem. C 114 (2010) 11977–11983.

[265] S. Chempath, B.R. Einsla, L.R. Pratt, C.S. Macomber, J.M. Boncella, J.A. Rau, B.S. Pivovar, Mechanism of tetraalkylammonium headgroup degradation in alkaline fuel cell membranes, J. Phys. Chem. C 112 (2008) 3179–3182.

[266] K.K. Chen, W. Salim, Y. Han, M. Gasda, W.S.W. Ho, Fluoride- and hydroxide-containing CO_2-selective membranes for improving H_2 utilization of solid oxide fuel cells, J. Membr. Sci. 612 (2020) 118484.

[267] L. Xiong, S. Gu, K.O. Jensen, Y.S. Yan, Facilitated transport in hydroxide-exchange membranes for post-combustion CO_2 separation, ChemSusChem 7 (2014) 114–116.

[268] Y. Wang, Y. Shang, X. Li, T. Tian, L. Gao, L. Jiang, Fabrication of CO_2 facilitated transport channels in block copolymer through supramolecular assembly, Polymers 6 (2014) 1403–1413.

[269] N.V. Blinova, F. Svec, Functionalized polyaniline-based composite membranes with vastly improved performance for separation of carbon dioxide from methane, J. Membr. Sci. 423 (2012) 514–521.

[270] P. Li, Z. Wang, Y. Liu, S. Zhao, J. Wang, S. Wang, A synergistic strategy via the combination of multiple functional groups into membranes towards superior CO_2 separation performances, J. Membr. Sci. 476 (2015) 243–255.

[271] M. Wang, Z. Wang, J. Wang, Y. Zhu, S. Wang, An antioxidative composite membrane with the carboxylate group as a fixed carrier for CO_2 separation from flue gas, Energy Environ. Sci. 4 (2011) 3955–3959.

[272] M. Wang, Z. Wang, S. Li, C. Zhang, J. Wang, S. Wang, A high performance antioxidative and acid resistant membrane prepared by interfacial polymerization for CO_2 separation from flue gas, Energy Environ. Sci. 6 (2013) 539–551.

[273] J.K. Yong, G.W. Stevens, F. Caruso, S.E. Kentish, The use of carbonic anhydrase to accelerate carbon dioxide capture processes, J. Chem. Technol. Biotechnol. 90 (2015) 3–10.

[274] M. Saeed, L. Deng, CO_2 facilitated transport membrane promoted by mimic enzyme, J. Membr. Sci. 494 (2015) 196–204.

[275] M. Saeed, L. Deng, Carbon nanotube enhanced PVA-mimic enzyme membrane for post-combustion CO_2 capture, Int. J. Greenh. Gas Con. 53 (2016) 254–262.

[276] K. Yao, Z. Wang, J. Wang, S. Wang, Biomimetic material—poly(*N*-vinylimidazole)–zinc complex for CO_2 separation, Chem. Commun. 48 (2012) 1766–1768.

Figure Captions

Figure 1. Experimental data of CO_2/N_2 separation and an empirical upper bound proposed by Robeson in 2008. Adapted from Ref. [51]; copyright Elsevier.

Figure 2. Effects of temperature on the predicted upper bounds for (a) CO_2/N_2, (b) CO_2/CH_4, (c) H_2/CO_2, and (d) CO_2/H_2. Adapted from Ref. [53]; copyright Elsevier.

Figure 3. Schematic of gas permeation through a facilitated transport membrane. Adapted from Ref. [77]; copyright American Chemical Society (ACS).

Figure 4. Binding geometries and energies of CO_2 and oligomers with various ether oxygen contents. Bond lengths are in the unit of Å. Key: C, gray; O, red; H, white. Adapted from Ref. [84]; copyright Elsevier.

Figure 5. Structure and CO_2/N_2 transport performance of poly(1,3-dioxolane) at 70°C. Adapted from Ref. [84]; copyright Elsevier.

Figure 6. Synthesis scheme of the cross-linked tris(2-aminoethyl)amine-poly(ethylene glycol) diacrylate membrane. Adapted from Ref. [121]; copyright ACS.

Figure 7. Synthesis of crosslinked poly(ionene) via the Debus-Radziszewski reaction. Adapted from Ref. [129]; copyright Elsevier.

Figure 8. Structures of commercial fluorinated polymers and perfluorodioxolane polymers.

Figure 9. Thermally rearrangement mechanism of (a) TR-α and (b) TR-β. Adapted from Ref. [153]; copyright Elsevier.

Figure 10. (a) Physical aging of a TR-α-PBO and its poly(hydroxyimide) precursor for 6 months; (b) Evolution of CO_2 permeance and CO_2/N_2 selectivity of a TR-α-PBO HF during physical aging and regeneration by methanol. Adapted from Refs. [165,166]; copyright Elsevier.

Figure 11. Schematic synthesis process of a crosslinked TR-α-PBO. Adapted from Ref. [170]; copyright Elsevier.

Figure 12. Synthesis of a TR-PBO copolymer containing Tröger's base units. Adapted from Ref. [176]; copyright Elsevier.

Figure 13. Synthesis of 6FDA-iptycene polyimides by using (a) triptycene and extended triptycene and (b) pentiptycene. Adapted from Refs. [182,183]; copyright Elsevier.

Figure 14. Hydroxyl-functionalized polyimides, derived from 2,2-bis(3-amino-4-hydroxyphenyl)-hexafluoropropane (APAF), containing conventional 6FDA and PIM-type 9,10-diisopropyl-triptycene dianhydrides (TPDA). Adapted from Ref. [196]; copyright Elsevier.

Figure 15. CO_2/H_2 selectivities and CO_2 permeabilities of FTMs containing 70 wt.% sterically hindered PAA and 30 wt.% crosslinked PVA at 110°C. Adapted from Ref. [72]; copyright Elsevier.

Figure 16. Interfacial polymerization of TMC and DNMDAm for the preparation of thin-film composite FTM. Adapted from Ref. [231]; copyright Wiley.

Figure 17. The carbamate pathways of (a) PZ-Gly and (b) PZEA-Sar and the bicarbonate pathways of (c) PZ-Gly and (d) PZEA-Sar for leading to their preferred products. Relative energies (ΔE, with respect to reactants) of structures in the amine–CO_2 reactions of carriers following the (e) carbamate and (f) bicarbonate pathways. Adapted from Ref. [241]; copyright ACS.

Figure 18. (a) Effect of CO_2 partial pressure on the CO_2 permeance of a FTM containing PZEA-Sar; adapted from Ref. [253]; copyright ACS. (b) Effects of membrane thickness on the CO_2 permeability and permeance of a FTM containing AIBA-K. Adapted from Ref. [254]; copyright Elsevier.

Figure 19. (a) ^{1}H NMR spectra of 0.5 M tetramethylammonium fluoride (TMAF) before and after heating at 130°C; (b) chemical shifts of water in the presence of 0.5 M of KF, CsF, and TMAF. Adapted from Ref. [266]; copyright Elsevier.

Figure 20. Transport properties of selected polymers against the (a) 2008 [51] and 2019 [52] CO_2/N_2 upper bounds, (b) theoretical CO_2/H_2 upper bounds at 25 and 120°C [53,81], (c) 2008 H_2/CO_2 upper bound [51] and its theoretical projection at 150°C [204], and (d) 2008 [51] and 2019 [52] CO_2/CH_4 upper bounds. Symbols: polyethers (✶); poly(RTIL)s (♦); perfluoropolymers (■); TR polymers (▲); iptycene-containing polymers (×); FTMs (●); PBIs at 35°C (►); PBIs at 150°C (★).